UNIVERSITEIT VAN PRETORIA
UNIVERSITY OF PRETORIA
YUNIBESITHI YA PRETORIA

ACHIEVING CONTROLLABLE CONTINUOUS VARIABLE DAMPING WITHIN A SEMI-ACTIVE HYDRO-PNEUMATIC SUSPENSION SYSTEM.

by

Benjamin de Wet

15334440

Submitted in partial fulfillment of the requirements for the degree

Masters of Engineering (Mechanical Engineering)

in the

Department of Mechanical and Aeronautical Engineering

Faculty of Engineering, Built Environment and Information Technology

UNIVERSITY OF PRETORIA

Monday 30th November, 2020

ABSTRACT

ACHIEVING CONTROLLABLE CONTINUOUS VARIABLE DAMPING WITHIN A SEMI-ACTIVE HYDRO-PNEUMATIC SUSPENSION SYSTEM.

by

Benjamin de Wet

Supervisor(s):	**Prof. P.S. Els**
Department:	Mechanical and Aeronautical Engineering
University:	University of Pretoria
Degree:	Masters of Engineering (Mechanical Engineering)

The compromise between ride comfort and handling for a passive suspension system is a well-known and often researched problem. Semi-active suspension systems offer significant improvements to this compromise. One example of a semi-active system, that can change both spring and damper characteristics between two discrete values is the 4-state semi-active hydro-pneumatic suspension system. This system can switch between a ”ride comfort mode” (soft spring and low damping) and a ”handling mode” (stiff spring and high damping) within $100ms$, improving both ride comfort and handling.

The discrete $4S_4$ could be improved upon further by adding continuous variable damping. Work on this topic showed great promise but also posed its challenges in achieving this in a safe and controllable manner.

In order to make continuous variable damping a reality a new configuration for the $4S_4$ is proposed. This new configuration incorporates a blow-off damper in parallel with a proportional flow control valve. The system ensures that, in the highly non-linear closing region of the proportional flow control valve, adequate damping for handling is maintained and uncontrollable peak pressure differences are avoided.

Experimental work conducted showed that the system was capable of achieving the required spring and variable damping characteristics in a safe and controllable manner. The experimental data was

used for parametrising and validating a physics based mathematical model of the suspension system. The mathematical model incorporates the: pressure drop *vs*. flow characteristics for both the blow-off and proportional valves, response time for the on-off valves as well as the gas pressure *vs*. flow characteristic incorporating the compressibility of the oil and thermal properties of the gas. This model can be used to make informed decisions on further prototype development or in full vehicle simulations.

The system makes continuous variable damping possible ranging from the optimal damping characteristic for handling to the low damping characteristic required for ride comfort. The system also shows a significant reduction in friction.

ACKNOWLEDGEMENT

Dedicating a small portion of one's career in pursuit of a masters degree can be rewarding and challenging at the same time. It comes to say that this journey does not come without its adversities. It is therefore important to ensure one is surrounded with a good support structure to uplift and help in the times when continuing in this pursuit seems impossible.

I would like to take this opportunity to extend my appreciation for everyone that shared in this journey with me:

- As the saying goes, you cannot choose your family... I would not have made any other choice. Thank you for your unconditional support and love in all my endeavours.
- I am very fortunate to have had the opportunity to tap into the vast knowledge of one of the front runners in the industry. Prof P.S Els thank you for your guidance and knowledge which you lent not only on an academic level.
- The dynamic nature and structure between the individuals in the VDG group makes going to the office an adventure. Thank you all for the part that each and everyone had.
- I would like to extend my appreciation for the long hours and hard work put in to manufacturing components and equipment for my experiments. Wietsche Penny and Glenn Guthrie thank you for your efforts. I also would like to thank all the staff of the heavy machine laboratory for their inputs.

It has been an incredible journey, one that I will always remember.

Table of Contents

Nomenclature

Roman Symbols

Symbol	Description	Unit
A	Area	m^2
A_0	BWR constant	$\left(\frac{m^3}{kg}\right)^3 \cdot \frac{N}{m^2}$
a	BWR constant	$\left(\frac{m^3}{kg}\right)^3 \frac{N}{m^2}$
B_0	BWR constant	$\frac{m^3}{kg}$
b	BWR constant	$\left(\frac{m^3}{kg}\right)^3$
C_A	Area coefficient	unit less
C_0	BWR constant	$\left(\frac{m^3}{kg}\right)^3 \cdot K^2 \cdot \frac{N}{m^2}$
C_d	Discharge coefficient	unit less
C_v	Velocity coefficient	unit less
Cv	Specific heat	$\frac{J}{KgK}$
c	BWR constant	$\left(\frac{m^3}{kg}\right)^3 \cdot K^2 \cdot \frac{N}{m^2}$
D	Diameter	m
$Disp$	Displacement	m
F	Force	N
K	Spring stiffness	$\frac{N}{m}$
L	Length	m
m	Mass	Kg
N_{1-9}	IG specific heat capacity constants	
$n; i$	Current data point	
P	Pressure	Pa
$Q; q$	Volumetric flow rate	$\frac{m^3}{s}$
R	Universal gas constant	$\frac{J}{KgK}$
T	Temperature	K
u	Fluid velocity	$\frac{m}{s}$
u_T	Theoretical fluid velocity	$\frac{m}{s}$
V	Volume	m^3
$\ddot{x}$	Acceleration	$\frac{m^2}{s}$
$\dot{x}$	Velocity	$\frac{m}{s}$
x	Displacement	m

Greek Symbols

Symbol	Description	Unit
α	BWR constant	$\left(\frac{m^3}{kg}\right)^3 \cdot \frac{N}{m^2}$
β	Bulk Modulus	Pa
Δ	Change in or difference between two states	
γ	BWR constant	$\left(\frac{m^3}{kg}\right)^2$
ρ	Density	$\frac{kg}{m^3}$
τ	Thermal time constant	$sec.$
ν	Specific Volume	$\frac{m^3}{kg}$
$\dot{\nu}$	Change in specific volume	$\frac{m^3}{kg \cdot s}$

Subscripts

Subscript	Description
0	Initial stage.
$1;2;3$	Identification of item when more than one present.
$1-2$	From position one to two.
$1-3$	From position one to three.
$1-3$	From position two to three.
$A_pBlow-off$	Blow-off point for the initial stage.
CVD	Continuous variable damping.
DaC	Double acting cylinder.
E	Effective orifice area.
frac	Fraction.
g	Gas.
l	Leakage area.
m	Final orifice stage of model.
p	Parallel orifice area.
proto	Prototype.
s	Series orifice area or temperature of surroundings.
v	Variable opening orifice area.
vfc	Valve Fully closed.
vfo	Valve Fully open.

List of Abbreviations

Abbreviation	Description
BS	British Standard
BWR	Benedict Webb Rubin
CVD	Continuous Variable Damping
CVV	Continuous Variable Valve
DAQ	Data Acquisition Computer
DT	Difference Threshold
EE	Energy Equation
IG	Ideal Gas
LVDT	Linear variable differential transformer
MR	Magneto-Rheological
RMS	Root Mean Squared
RRMS	Running Root Mean Squared
SUV	Sports Utility Vehicle
$4S_4$	4-State semi active suspension system
$4S_4CVD$	4-State semi active suspension with continues variable damping

List of Figures

1. Introduction

1.1 Background

In designing a vehicle's suspension there is always a compromise between ride comfort and handling (Els 2006). Generally speaking, ride comfort requires a soft suspension with low damping and handling requires a hard suspension with high damping. Savaresi et al. (2010) includes various studies focused on finding the optimal performance for a semi-active suspension in terms of ride comfort and handling. These studies conclude that there is a clear compromise between optimal road holding ability and ride comfort. Thus, with a passive suspension system, achieving optimal ride comfort and optimal handling is not possible due to the two requirements being at two different regions of the design space.

A similar problem arises when one would consider a freight carrier or haul truck. The optimal suspension characteristics required for a full and empty load is vastly different.

Els (2006) recognised this compromise and presented a solution in the form of a 4-State Semi-active hydro-pneumatic suspension system ($4S_4$). The system presented by Els solved the need to make a compromise between handling and ride comfort for a vehicle's suspension system by changing between the settings depending on the conditions experienced by the vehicle. However only two states of the four were investigated: Soft spring with low damping (for ride comfort) and a hard spring with high damping (for handling). Employing a $Running - RMS$ control strategy, the $4S_4$ is capable of switching between handling and ride comfort mode with a system response time of less than $100ms$.

Following on Els's work, Vosloo (2018) attempted to realize a version of the $4S_4$ that is capable of achieving continuously variable damping. Vosloo build only one halve of his proposed configuration but was able to achieve excellent correlation between experimental data and a model for a semi-active hydro-pneumatic continuous variable damping suspension system. As part of his model Vosloo (2018) considered the following to achieve this good correlation:

1. The friction characteristic of the $4S_4CVD$.
2. The pressure drop vs. flow characteristics for the flow controlled solenoid valve.
3. Compressibility of the oil.
4. Valve response times.

5. The BWR real gas model with the energy equation to calculate the pressure in the accumulator.

By using a flow control solenoid valve, Vosloo's work showed great promise of achieving a full semi-active suspension system with continuous variable damping. Although Vosloo was able to characterise and model the different components of the $4S_4CVD$, his analysis indicated that the proposed architecture is not feasible due to the high non-linearity of the valves which makes it difficult to control the pressure drop accurately in the closed region of the valve's operation. The spring and damper characteristics were also strongly coupled since the same valve controlling the flow for damping also closed off the accumulator to sustain the spring characteristic.

1.2 Research Objective

The objective of this research study is to develop a new architecture of the $4S_4$ that will be capable of achieving continuous variable damping while incorporating blow-off characteristics.

A mathematical model of the new proposed configuration, building on previous proven solutions, that includes all the aspects that are needed for good correlation with experimental results of the physical system, is developed. This mathematical model must be computationally efficient so that it can be employed in full vehicle simulations as well as aiding in the improvement of further possible prototypes. The mathematical model is validated against a manufactured prototype. Although the design and development of the suspension hardware formed part of this study, the documentation of the design and manufacturing process followed however do not fall into the scope of this document.

1.3 Document Layout

This document consists of 6 chapters:

- **Chapter 1 Introduction:** Introduction and background into the development of this research objective.
- **Chapter 2 Literature Study:** More in-depth information from literature is considered on the research topic as well as relevant information required in later chapters.
- **Chapter 3 Experimental Set-Up:** Hardware, data capturing and experimental set-ups that was used to obtain data is described in this chapter.
- **Chapter 4 Mathematical Models:** The mathematical modelling process followed to model the proposed configuration based on the literature.

- **Chapter 5 Full Architecture & Model:** The development of a prototype allows for validation of the mathematical models. The functionality of the proposed architecture is also considered
- **Chapter 5 Conclusions and Recommendations:** Concludes the research study and make recommendations for future work.

2. Literature Study

This chapter will introduce the ride comfort *vs*. handling compromise as well as the solutions under investigation. Detailed blow-off damper modelling will be investigated as well as physics based modelling of the complete suspension system.

2.1 The Compromise Between Ride Comfort and Handling

Gillespie (1992) states that the occupant of a vehicle will experience the broad range of vibrations, associated with vehicle road interface as well as vehicle mechanical vibrations, through three paths: visual, aural and tactile. The term ”ride comfort” is used to describe human response to tactile vibrations in a vehicle. Ride comfort will be experienced differently when perceived by different occupants. The perception of ride comfort is closely related to the acceleration experience by the human. Another complexity added to ride comfort classification is the fact that the human body experiences different frequencies of vibration differently, due to the fact that the human body is more sensitive to some frequencies than others. Hence the classification of ride comfort needs to account for this to quantify how the occupant of a vehicle will experience the ride.

The *BS*6841 standard (BritishStandardsInstitution 1987) is widely used for ride comfort evaluation. This standard makes use of a weighting function to weigh the acceleration in the frequency domain according to human perception to vibration. The vertical direction is often considered to dominate and many studies only focus on this direction in quantifying the ride comfort. The weighting curve, for the vertical direction, is presented in figure 2.1 as set up according to this standard. Note the change in sensitivity throughout the frequency range.

After the vibration signal is weighed the RMS of the signal is computed and used as a measure of the ride harshness. Thus, for the ride comfort of the vehicle, the suspension must isolate the occupants from the vibration that the vehicle is subjected to. This generally requires large suspension travel with low damping and spring forces on rough terrains. The suspension system natural frequency should also avoid the $4-8Hz$ range where the human is most susceptible to vertical vibration. For this reason, the sprung mass natural frequency is usually around $1-2Hz$ and the unsprung mass natural frequency $>10Hz$.

The handling of a vehicle is determined by the lateral, yaw and roll dynamic response to a steering input (Gillespie 1992). Generally handling requires a stiff suspension to limit body roll. To ensure tyre-road contact, high damping and a stiff spring is required.

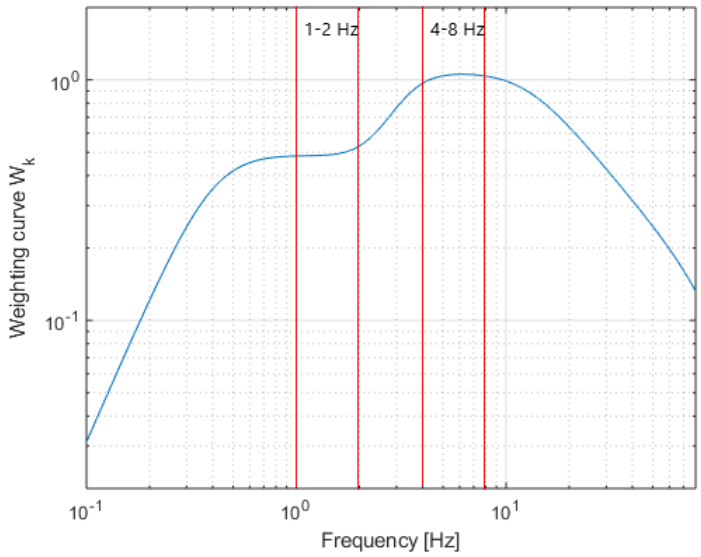

Figure 2.1. *BS*6841 frequency weighting ride comfort evaluation.

With a passive suspension system, it is challenging to find a good compromise between handling and ride comfort. Ride comfort and handling requires two different suspension set-ups that cannot be achieved with a single passive suspension set-up without some sort of compromise.

2.1.1 The need for variability in damping

The effect that a continuous variable damper, controlled by an ideal skyhook control algorithm, have on the body acceleration, vertical displacement and suspension deflection for a certain road input was investigated by Ahmed et al. (2019). In this numerical analysis a $\frac{1}{4}$ car model was used to compare the continuous variable damper with a passive damper as well as a semi-active damper that adapts the damping characteristics depending on body velocity and relative suspension velocity by switching between 2 discrete damping coefficients controlled by an on-off shyhook control strategy.

Simulation results (Ahmed et al. 2019) showed that the continuous variable damper was able to reduce the vertical acceleration of the sprung mass with 73.4% when compared to the passive damper and 53.8% when compared to the on/off semi-active damper as can be seen in figure 2.2. Both vertical displacement and suspension deflection also saw a reduction for the continuous variable damper in comparison to the other two systems.

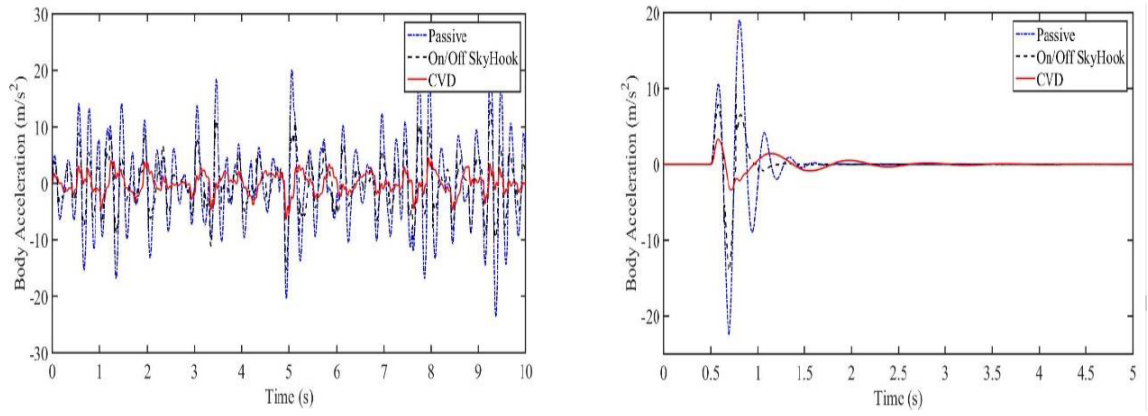

Figure 2.2. Quarter car simulation results for vertical acceleration comparing 3 suspension set-ups (Ahmed et al. 2019).

Jugulkar et al. (2016) showed that to obtain constant damping performance it is essential to vary damping characteristics. By employing a validated continuous variable damper model in quarter car simulations Jugulkar et al. (2016) showed that it is possible to obtain a 15% improvement in sprung mass acceleration transmissibillity and a 10% handling improvement if compared to a passive suspension.

Experiments conducted by Sha et al. (2020) showed that a semi-active suspension system with a continuous variable magnetorheological damper controlled with a linear quadratic Gaussian control algorithm is superior over a traditional passive suspension on various performance indexes. The experiments showed that the semi-active system employing continuous variable damping improved ride comfort, safety and stability of the vehicle.

2.1.2 Optimal damper characteristic

Thoresson (2007) did optimization work on the suspension characteristics needed for handling and ride comfort for a Land Rover Defender 110. The damping force was approximated using 6 design variables to account for compression and rebound damping, the low and high velocity characteristic and the location of the knee point.

The results for handling are presented in figure 2.3. This is a theoretical characteristic and may not necessarily be feasible to achieve physically in damper design. This is, however important, as this result will ensure optimal handling and needs to be considered in the design of the dampers.

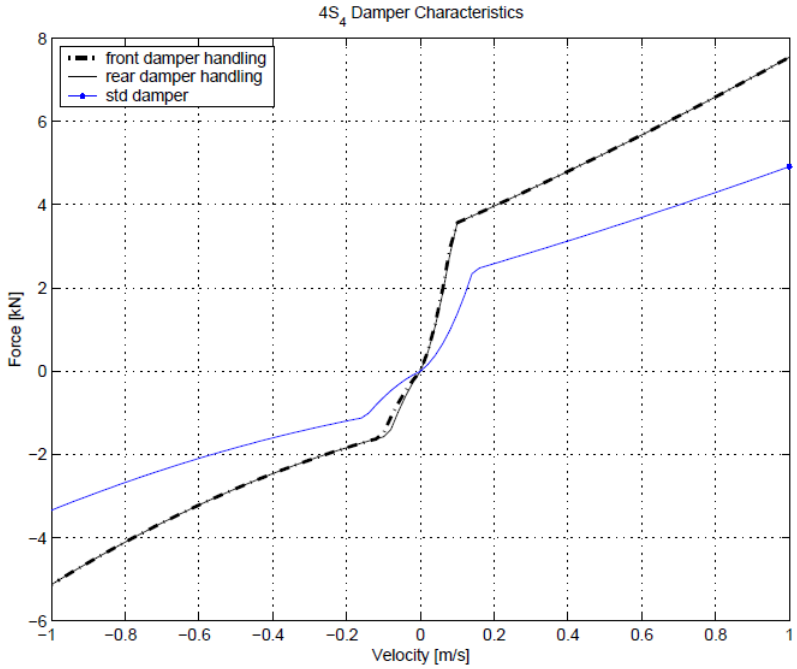

Figure 2.3. Optimized damper characteristics for handling (Thoresson 2007)

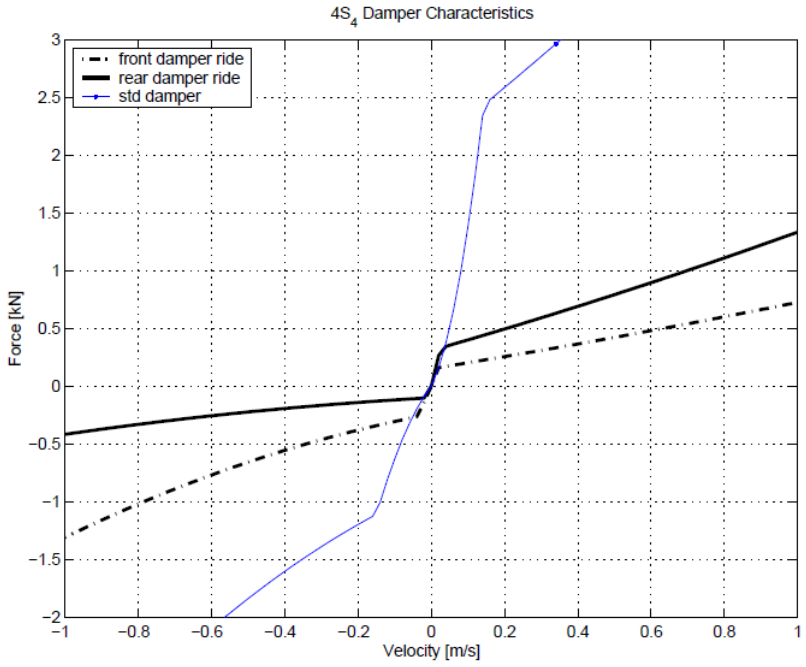

Figure 2.4. Optimized damper characteristics for ride comfort. (Thoresson 2007)

2.2 Hydro-Pneumatic Semi-Active Suspension

2.2.1 The 4-state semi active suspension ($4S_4$)

Els (2006) determined that for a suspension system to eliminate the compromise between ride comfort

and handling, it requires at least 2 characteristics. One characteristic must have a soft spring and low damping for ride comfort, and another characteristic that has a hard spring and high damping for handling. This led to the development of the $4S_4$, so-called because of its ability to achieve 4 suspension characteristics/states. This is possible due to 2 spring settings and 2 damping settings that can be combined with the switching of solenoid valves.

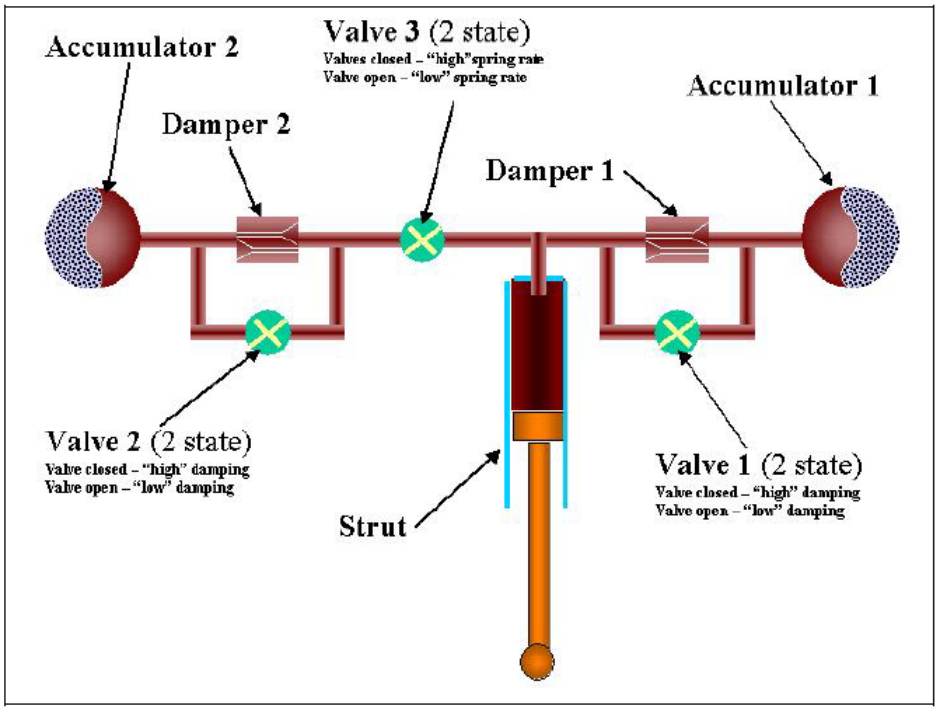

Figure 2.5. 4S4 Architecture (Els 2006).

Figure 2.5 depicts the circuit layout of the $4S_4$. The $4S_4$ consists of 2 gas accumulators, with a combined accumulator volume of $0.5l$ for ride comfort and $0.1l$ for handling. By opening and closing valve 3 either both accumulators are used, or only accumulator 1 is used for the selection between a soft and hard spring. The $4S_4$ is capable of high damping, making use of blow-off damper packs, and low damping, by bypassing the damper packs. This is achieved by opening and closing valves 1 & 2, to force flow through the damper packs or to by-pass the damper pack through the relevant channels.The $4S_4$ is thus capable of four states, with the following possible combination of spring and damper settings:

- Soft spring & soft damper.
- Soft spring & hard damper.
- Hard spring & soft damper.

- Hard spring & hard damper.

The characteristics for the spring and damping force for the $4S_4$ is depicted in figure 2.6. Note that the original damping curve for the Land Rover Defender 110 (vehicle of implementation) is also presented for comparison.

The $4S_4$ provides a "ride comfort mode" (soft spring and low damping) and "handling mode" (hard spring and high damping). The ride comfort *vs* handling compromise is solved by employing a suitable control strategy that can switch the system between “ride comfort mode” or “handling mode”. Els (2006) implemented the $4S_4$ on a Land Rover Defender 110. Conducting various tests, Els (2006) was able to show that the $4S_4$ does indeed improve the handling of the vehicle with $61-78\%$ if compared to the baseline suspension. The ride comfort improvement grained by switching from “handling mode” to “ride comfort mode” was $50-80\%$.

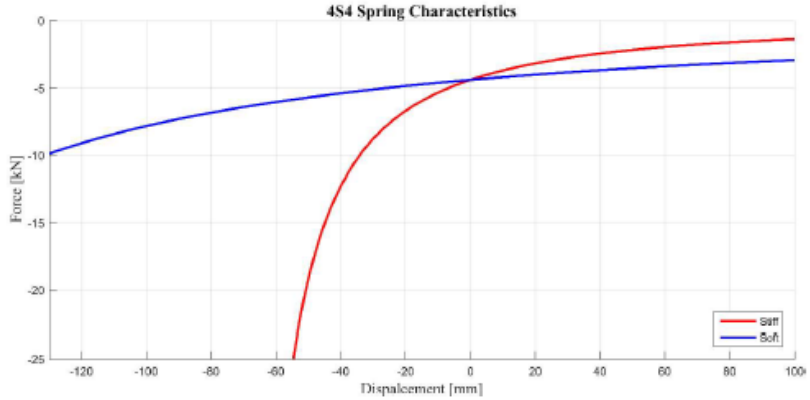

(a) Spring Force.

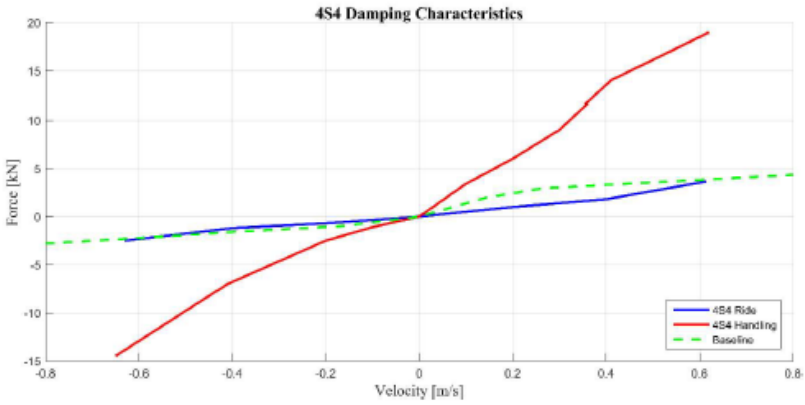

(b) Damping characteristics

Figure 2.6. $4S_4$ characteristics generated from a mathematical model. (Els 2006)

2.2.2 Continuous variable damping semi-active suspension

After successful implementation of the $4S_4$, investigations were conducted to incorporate continuous variable damping. Meeser (2015) & Grobler (2016) investigated the use of magneto-rheological technology to achieve variable damping. However, Heymans (2017) concluded that the MR equipped $4S_4$ can not be further improved to meet all the requirements for a sufficient continuous variable damper, mainly due to the characteristic of the MR fluid under the high pressure experienced in a hydro-pneumatic suspension system.

An alternative approach to achieve continuous variable damping by using two proportional valves, one Normally open and one normally closed, was investigated byVosloo (2018). Vosloo set out to characterise and model a version of the $4S_4$, that will allow continuous variable damping. The architecture is depicted in figure 2.7.

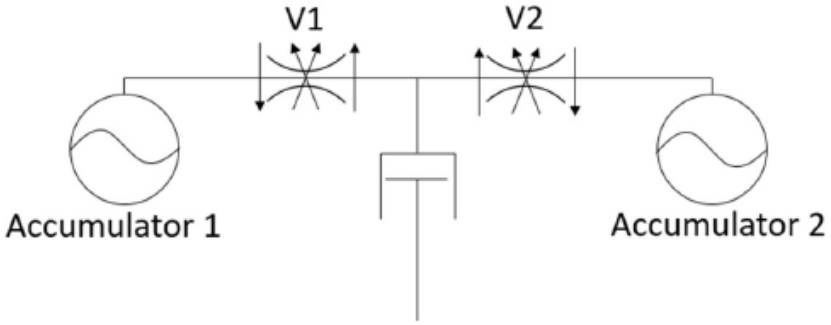

Figure 2.7. $4S_4CVD$ Architecture (Vosloo 2018).

The $4S_4CVD$ is based on the design of the original $4S_4$, but changes were made that include:

- **Valves:** The on/off valves used in the $4S_4$ were replaced with proportional flow control servo valves. These valves make it possible for variable flow restriction, causing either more or less damping.
- **Spring Characteristics:** The set-up as depicted in figure 2.7 allows for 4 discrete spring characteristics. By controlling the 2 valves the following combination between the accumulators, and hence "spring stiffness's" are possible:

  1. Only accumulator 1.
  2. Only accumulator 2.
  3. Accumulator 1 and 2.

4. "Locked" closing both valves. This will allow for only the compressibility of the oil and hence a very stiff spring.

- **Piston diameter:** The piston diameter of the $4S_4CVD$ was reduced from the $50mm$ of the $4S_4$ to $32mm$. This has the advantage of reducing package size and also decreasing the induced flow rate by the movement of the piston. This will allow for lower damping to be possible using the same valves.
- **Friction:** The floating pistons of the $4S_4$ gas accumulators were replaced with rolling diaphragms in an attempt to reduce the friction.
- **Ride height:** The $4S_4CVD$ makes use of two additional flow control valves to include ride height control or the possibility of cross-linked suspension. The original $4S_4$ also had this capability with the use of on/off valves. Note: ride height control valves not indicated in any of the architectures considered, nor is it considered in this study.

The design considered by Vosloo (2018) is depicted in figure 2.8

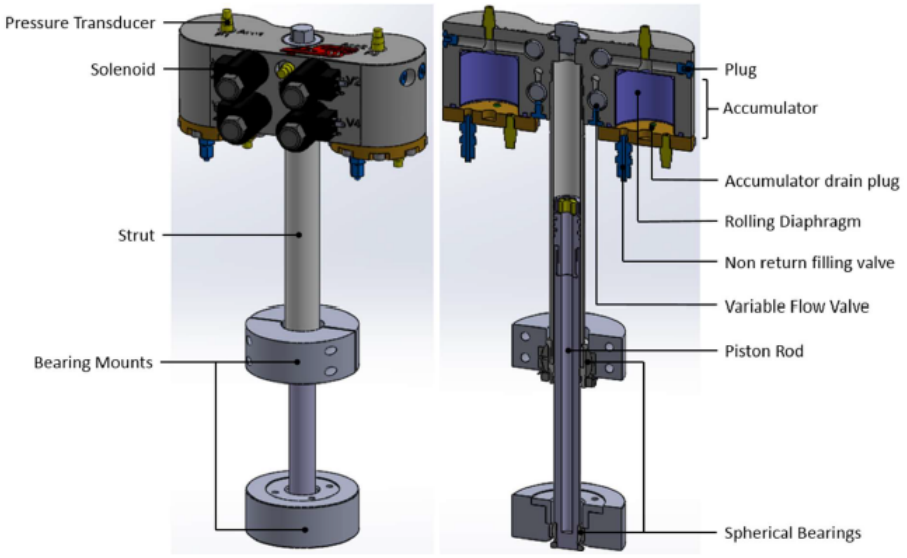

Figure 2.8. $4S_4CVD$ Design. (Vosloo 2018)

Vosloo (2018) did extensive work on characterising the components used for one half of the $4S_4CVD$. In the modelling process, Vosloo found that the current driver, used initially, for the solenoid control valves was insufficient in producing the response time needed for a semi-active suspension system ($< 100ms$ as recommended by Els (2006)). After some improvement of the current driver, the valves were able to respond in adequate time.

Vosloo (2018) extracted the damping characteristics of the flow controlled solenoid valves experimentally, presented in figure 2.9. From this result, it was clear that the low damping will be significantly lower than that of the $4S_4$. The low damping characteristic of the $4S_4$ was higher than the optimal characteristic required for ride comfort (Els 2006). It is also clear that the higher damping will at least produce the same amount of damping as the $4S_4$ high damping state, refer back to figure 2.6(b) for comparison.

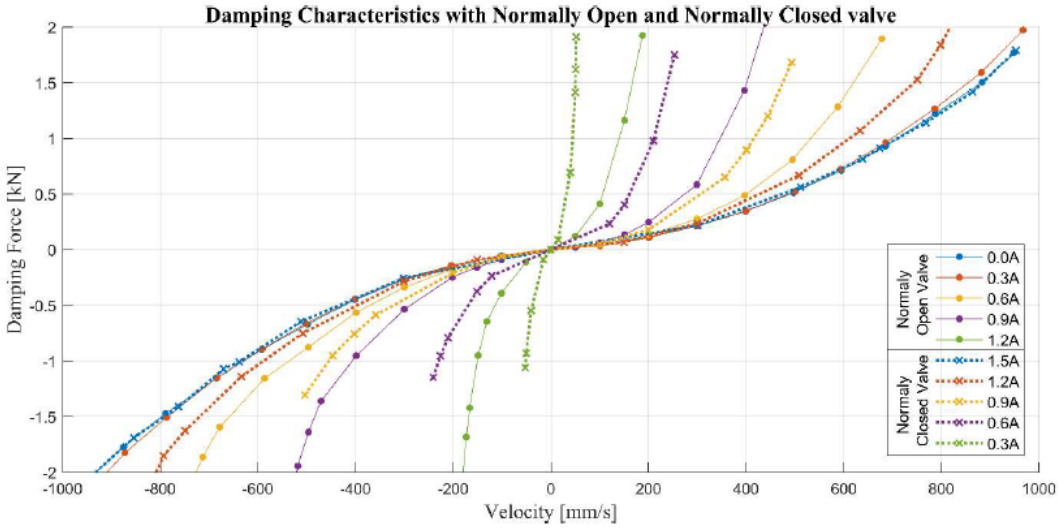

Figure 2.9. $4S_4CVD$ Damping characteristics for both the normally open, and -closed valves. (Vosloo 2018)

From Vosloo (2018) it is clear that by using the flow controlled solenoid valves, it is possible to achieve sufficient variable damping. It was also shown that modelling such a damper is possible to a high degree of accuracy if all the aspects are considered. Vosloo's work sets a new perspective and possibilities for changing the configuration of the $4S_4$, to achieve a suspension system that is capable of achieving continuous variable damping within the needed parameters for a semi-active suspension system. The architecture presented by Vosloo was however not feasible. The problem arose due to the high non-linearity when approaching the closed position of the valve. This would not only increase damping , but also simultaneously block the accumulator resulting in a rapid increase in stiffness. This may lead to a sudden lock-up of the suspension accompanied by highly uncomfortable ride and reduced handling ability.

The logical solution to this problem is to add a blow-off damper in parallel to the proportional flow control valve. This new architecture will be proposed in section 2.6.2. The design and modelling of this blow-off damper valve will now be considered.

2.3 Damper Design

2.3.1 The orifice

The basic fundamentals for the operation of a hydraulic damper are based on that of fluid flowing through an orifice. Orifice flow is a well-understood topic in literature and can become extremely complex, quickly. However, for the practical application in damper design the focus will be on the fundamental understanding of the pressure drop over and flow through an orifice.

Dixon (2007) presents the volumetric flow rate through an orifice as follows:

$$Q_{orifice} = C_d \cdot A \cdot u_T \tag{2.1}$$

With the variables representing:

1. **Effective exit area(A):** The effective area of the orifice is expressed as $A_E = C_A A$. Where C_A represents the ratio of the area relating to the orifice and the *vena contracta*. For high Reynolds numbers, C_A can be calculated, but in practical damper applications, this value is normally observed($C_A = 0.8$ was observed as a reasonable estimate Dixon (2007)).
2. **Theoretical velocity(u_T):** This velocity is calculated using the Bernoulli equation, but this is purely theoretical. The actual velocity can be calculated as $u = C_v u_T$ where $C_v = \frac{mean_{velocity}}{Ideal_{velocity}}$. This however requires that the actual velocity is known through the orifice.

From equation 2.1 it is clear that the *Discharge coefficient(C_d)* is the product of the velocity and area coefficients:

$$C_d = C_v C_A \tag{2.2}$$

The accuracy of equation 2.1 depends on how accurate the C_d can be determined. The C_d is affected by the Reynolds number of the fluid flow. For this reason, the C_d can be an array of values depending on the operating conditions of a damper, seeing that a vehicle can be subjected to various road inputs at different velocities. Segel & Lang (1981) showed that a useful first approximation for C_d is 0.7.

As shown by Lichtarowicz et al. (1965) for most practical damper applications, the Reynolds number is too high for the C_d to be only a function of the Reynolds number. The discharge volume is therefore primarily dependent on the density, with moderate influence from the viscosity, and is being accounted for with the discharge coefficient. The analysis was done for short tubes ($\frac{L}{D} \leq 10$) with turbulent or laminar flow.

2.3.1.1 Accounting for the variations in C_d

Seeing that the Reynolds number for the fluid flow changes, it is necessary to consider this change in the design of the orifice and the determination of the C_d value. A good design should keep this variation as small as possible.

Mcgreehan & Schotsch (1988) showed that by rounding and chamfering the geometry of the orifice, improvements in the discharge coefficient is achievable. However this only accounts for the effects of the geometry and not for the Reynolds number, hence the simplified C_d value by Segel & Lang (1981). For this reason, the following design considerations are necessary for orifice design:

1. Performance variation must be built into the accepted design requirements.
2. High tolerances on the components can minimize the variations in performance.
3. Individual components can be calibrated by flow measurement experiments.
4. The design requirements can be adapted to reduce the sensitivity in variations.

2.3.1.2 Orifices in series and parallel

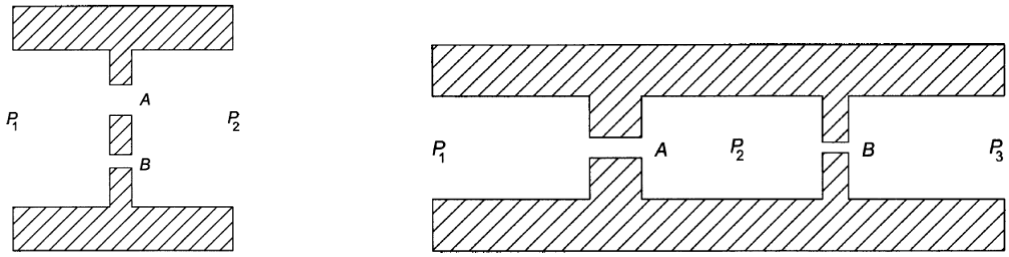

(a) Parallel orifices. **(b)** Series Orifices.

Figure 2.10. Cascading Orifices configurations.

Orifices can be cascaded in order to obtain a combined effect of two or more orifices. These configurations can be either in parallel or in series as depicted in figure 2.10. For these configurations, the flow rate and pressure drop over the orifices can be determined as follows:

- **Parallel Orifices:** For orifices in parallel the flow rates are simply added:

$$Q_{total} = Q_A + Q_B \tag{2.3}$$

- **Series Orifices:** For orifices in series with steady flow the continuity equations requires that the flow rate is constant and hence the sequential pressure drop is added together. Considering the

two series orifices in figure 2.10(b):

$$P_{1-3} = P_{1-2} + P_{2-3} \tag{2.4}$$

2.4 Valve/Damper Models

Numerical modelling of dampers follow one of two approaches:

1. Parametric approach or
2. Physical approach.

Parametric modelling is a black box approach (Leser et al. 2002). The advantage of this approach is that machine learning can be employed to recognize dependencies between inputs and outputs (Castellani et al. 2017). These models however lack in practical and conceptual understanding of the functioning behind a damper. A variation, gray box model, is proposed by Beghi et al. (2007). Certain aspects like the friction and hydraulic forces are based on physical modelling while the hysteresis effects are modelled with artificial neural networks.

The physical approach calculates the pressures based on the geometry of the damper and parameters that includes oil inertia, oil compressibility, mechanical compliance of chambers and seals. Initial physical modelling attempts (Lang 1977) included 80 parameters. This number was later reduced to 14 by Reybrouck (1994). Recent developments (Duym 2000) includes the dynamics of the flow across the valve. Alonso & Comas (2006) presented a new physics based mathematical model for a twin tube shock absorber that enables a better understanding why physical phenomena, like cavitation, takes place in the operation of a damper.

Dixon (2007) presents a combination of orifices to account for different aspects as indicated in figure 2.11. This combination of orifices is used to achieve a physics based mathematical representation of the required characteristics of a vehicle's damper as in reality. This can be built into a mathematical model deliberately to account for specific aspects in the damper being modelled. The different orifices in figure 2.11 represent the following:

- A_p**:** This represents the parallel orifice area. This is in parallel to the primary orifice area. In this case, the variable orifice area in combination with the series orifice area. This area is usually incorporated to ensure that the pressure between P_1 and P_3 equalises for low damper speeds.
- A_s**:** Series orifice area. This area is in series with the variable area and the leakage area.

- A_l**:** This represents the orifice area that will account for any leakages in the system. This can be included to model worn dampers or any other possible leakages in a damper design.
- A_v**:** This area models an orifice that can be opened in a variable manner. This area is normally activated if the pressure P_2 is greater or equal to the pressure required to open the valve denoted by P_{vfc}. This area will gradually open until the valve is fully opened at the pressure denoted by P_{vfo}. The opening of this valve can be linear but will be determined by the kind of opening mechanism used in the damper design (e.g. linear spring, Belleville spring or shim stacks).

Hence Dixon (2007) showed that complex damper designs could be mathematically modelled by combining orifices is series and parallel with typical mechanical components found in damper designs. However, with added complexity, the need for computational power also grows and needs to be considered in the mathematical modelling of a damper.

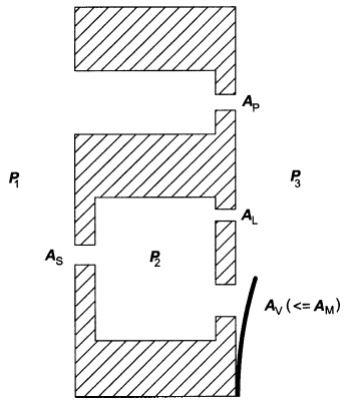

Figure 2.11. Representation of valve areas and pressures (Dixon 2007).

2.4.1 Valve adjustments

Considering the valve as depicted in figure 2.11 the adjustment of the various orifices and variability of the variable valve will be presented in this section as presented by Dixon (2007). The means of achieving the adjustability of each component is not the focus, but rather the effect of adjusting the various components and how this will feature in the $P(Q)$ function/curve of the model.

Dixon (2007) modelled the damper in figure 2.11 with a certain characteristic suitable to illustrate the effects as depicted in figure 2.12. To illustrated the effect Dixon (2007) reverted back to the same base characteristics while adjusting/varying the parameter of concern.

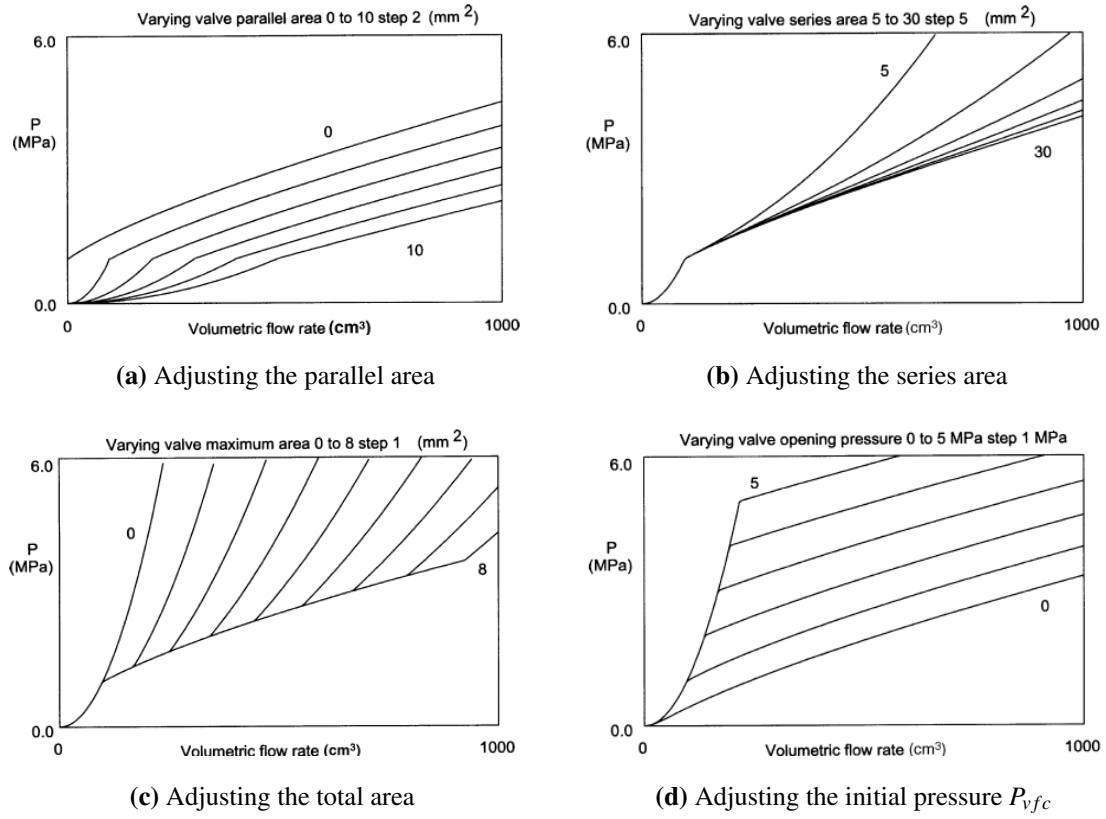

(a) Adjusting the parallel area

(b) Adjusting the series area

(c) Adjusting the total area

(d) Adjusting the initial pressure P_{vfc}

Figure 2.12. Effect of adjusting the various components of an adjustable valve. (Dixon 2007)

2.4.1.1 Parallel orifice area

The adjustment of the parallel orifice area has an effect over the entire flow rate region of the valve. Given the quadratic nature of the flow rate as set out in equation 4.1, the effect of varying this area will either increase or decrease the parabola shape. Hence moving stage 1 earlier or later in the flow regime as seen in figure 2.12(a) and also increasing the total orifice area once the valve is fully open.

2.4.1.2 Series orifice area

Adjusting the series orifice area will affect stages 2 & 3 of the valve. The adjustment of this orifice area is highly non-linear, figure 2.12(b), therefore care should be taken when incorporating this in a damper design. Dixon (2007) states that adjustability of this nature has been achieved on at least one damper design.

2.4.1.3 Total orifice area

Changing the area of the variable orifice (A_v) will only affect stage 3 as can be seen in figure 2.12(c). This adjustment will determine at what flow rate stage 3 will begin. If the flow rate is too low for the

valve to be fully open, then no effect will be seen for this adjustment.

2.4.1.4 Valve opening pressure P_{vfc} (Pre-load)

According to Dixon (2007) this is a well-established method of control for an adjustable damper. Increasing the pre-load will have no effect on stage 1 & 3. This will, however, determine the range in which stage 1 is active and defer the beginning of stage 3 accordingly. By increasing the spring pre-load, the pressure at which stage 2 is activated is increased and shifts this point up or down vertically as can be seen in figure 2.12(d).

2.4.1.5 Transition stage gradient

The adjustment of stage 2 can be achieved by varying the stiffness of the mechanism used for the variable opening of the valve. This kind of adjustability may not always be practically achievable but will allow for the design of a suitable damper characteristic. For instance by changing the stiffness of the spring used in the variable opening of the orifice area A_v it will allow the gradient of the transition stage to be adjusted either to a steeper gradient or to decrease this gradient. This does not affect stage 1 or stage 3 except for the fact that the beginning of stage 3 will be either delayed or advanced.

2.5 Modelling Methodology of a Semi-Active Hydro-Pneumatic Suspension System

2.5.1 Hydro-pneumatic spring

The spring force produced by the $4S_4$ is generated by compressing nitrogen gas. It is thus expected that the spring force can be calculated with gas laws. Van der Westhuizen & Els (2015) investigated the use of 5 different gas models to calculate the force produced by the hydro-pneumatic spring. In this investigation Van der Westhuizen & Els (2015) considered:

- three variations of the IG (Ideal Gas) law namely:
  - Isothermal process.
  - Adiabatic process.
  - IG law in conjunction with EE (Energy Equation).
- The other two models employed the BWR (Benedict Webb Rubin) real gas equations:
  1. With a temperature update using the EE and
  2. Keeping the temperature constant.

In this investigation, Van der Westhuizen concluded that, because of the significant temperature change of the gas, it is best to use a real gas model that incorporates heat transfer using a thermal time constant approach, instead of using a single polytropic exponent.

The best results in accordance with experimental data were with the use of the BWR gas model with incorporating the EE to calculate the gas temperature. Els (2006) stated that the typical pressure and temperature conditions of the hydro-pneumatic spring allows for the use of the BWR model.

Els (2006) found that by assuming the hydraulic fluid to be incompressible and only calculating the specific volume based on the amount of mass in the accumulator lead to significant errors. The changing of the specific volume must take the compressibility of the fluid into account for an accurate representation.

2.5.2 Flow split

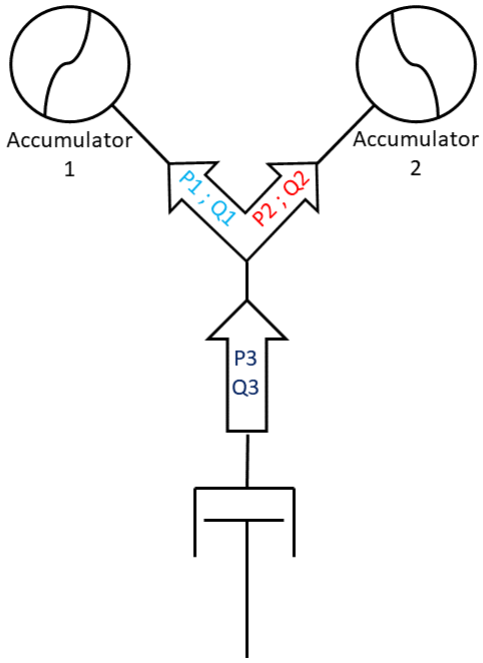

Figure 2.13. Flow split illustration diagram

Considering the $4S_4$ as depicted in figure 2.5. If valve 3 is open, then the flow is divided between accumulators 1 & 2. Similarly with the $4S_4CVD$ as depicted in figure 2.7 if the valves $V1$ and $V2$ is both partially or fully open the flow no longer flows to only one accumulator, but divides according to the pressure drop over the valves and pressure of the accumulator.

Vosloo (2018), as well as Theron & Els (2007) modelled the flow split, solving for the fraction of flow to each accumulator with a numerical method. However, due to the highly non-linear complex nature of the system, it was found by Heymans (2017) that using this approach the sampling frequency ($1000Hz$ - $2000Hz$) is important for accurate approximations. Heymans also stated that applying large velocity inputs will have detrimental effects on the approximation. From this, it is clear that to include the flow split in simulation is computationally expensive and not always feasible, for this reason, simulations were typically conducted either with one accumulator or both accumulators already in equilibrium as done by Vosloo (2018).

2.5.3 Friction

Van den Bergh (2014) investigated different friction models and the effect that it will have in modelling it in the $4S_4$ on vehicle dynamic simulations. Van den Bergh found that neglecting a friction model, especially for high friction, in the simulation has a significant impact on the accuracy of the simulation. He also stated that the high computational cost of a complex friction model does not outweigh the additional accuracy if compared to a simple experimentally determined look-up table.

Vosloo (2018) extracted the friction characteristics for the one half of the $4S_4CVD$ experimentally. The friction was characterized with the accumulator at a charge pressure of $7MPa$. This was done to minimize the pressure-dependence effects on the friction characteristics. The friction characteristic is presented in figure 2.14, along with the characteristic obtained by (Van den Bergh 2014) for the $4S_4$.

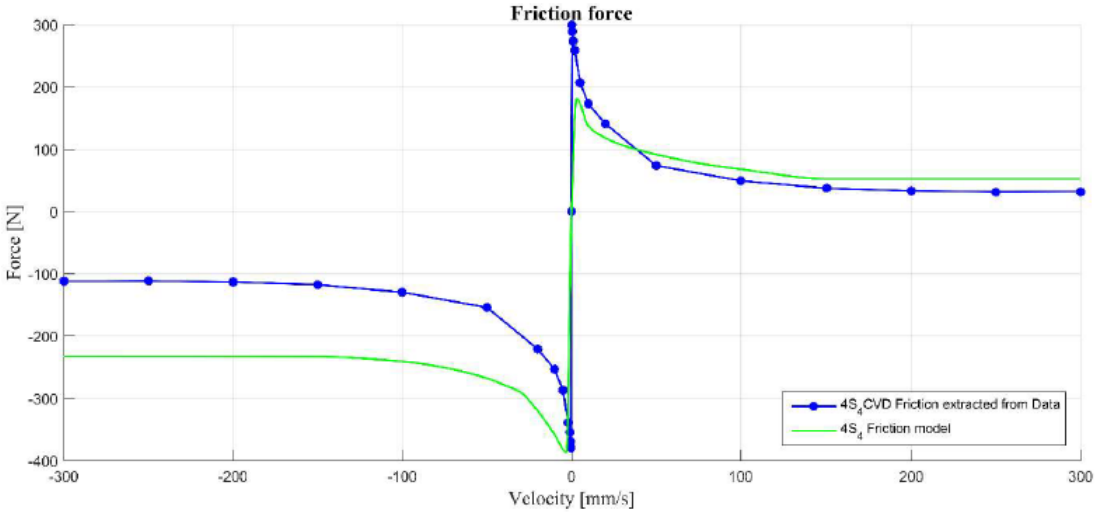

Figure 2.14. Friction characteristic of the $4S_4CVD$ (Vosloo 2018).

Also presented in figure 2.14 is the friction model of Van den Bergh (2014) for comparison. It is clear from the figure that Vosloo's design does indeed reduce the friction. However, stick/slip friction is still quite dominant and will affect the performance of the system.

2.5.4 Response time

When modelling the transients of the system, it is important to include the response time of the valves. Both Els (2006) and Vosloo (2018) did extensive experimental work to determine the response time of the various valves. It was found that the response time is dependent on the pressure drop over the valves. Vosloo concluded that to determined the response time accurately, a more controlled environment was needed. He stated that the results he obtained might be sufficient to analyse the performance of the $4S_4CVD$.

The pressure-dependent valve time delays is presented in figure 2.15. These time delays are important in creating a model that will represent a system that might use these valves.

2.6 Conclusion of Literature Review

The known compromise between handling and ride comfort in suspension design was shown. A solution to this compromise was presented ($4S_4$ developed by Els (2006)). The need for variable damping was presented as well as work done on the $4S_4$ to try and incorporate variable damping into the design. The literature review also presents the optimal damping characteristic that needs to be achieved for handling and ride comfort.

A mathematical model can be developed, taking into consideration experimental work and findings from previous systems, to represent the proposed configuration it should include: a gas model making use of the EE and considering the compressibility of the oil, friction characteristics of the unit, flow split and the response time of the valves. It was also shown that the blow-off valve can be modelled using a physics based modelling technique that can represent the different stages of the valve. This model can then be used in the design process to further improve the possibility of achieving a system that will allow the realisation of continuous variable damping.

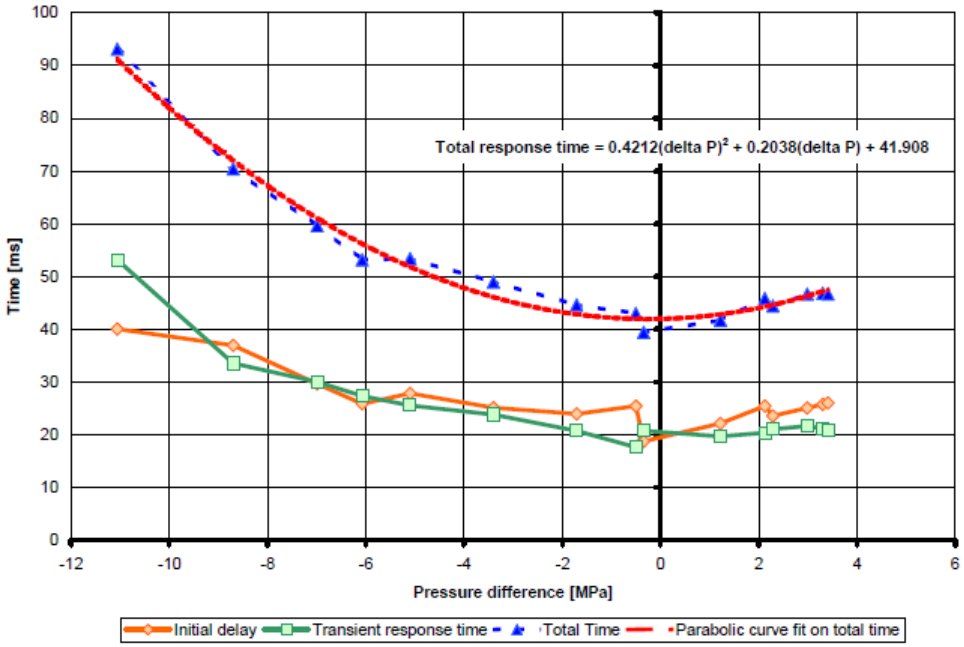

(a) On-off valve used in the $4S_4$. (Els 2006)

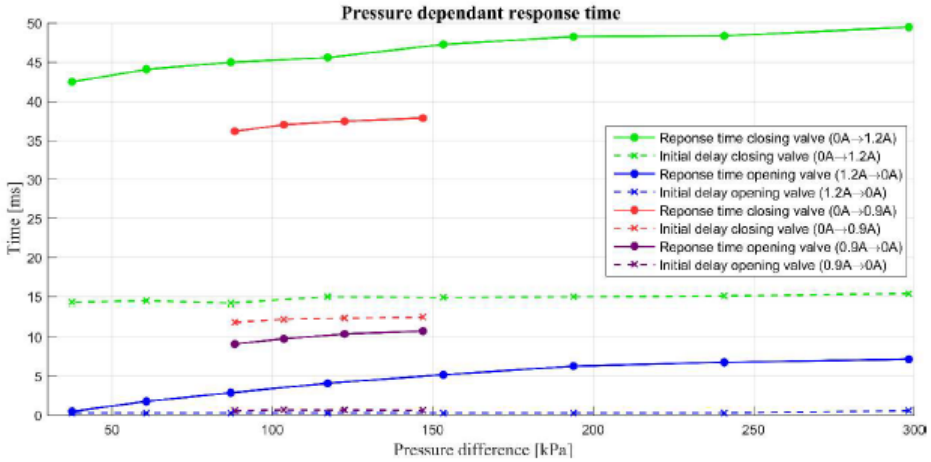

(b) Proportional flow controlled valve used in the $4S_4CVD$. (Vosloo 2018)

Figure 2.15. Time delays for the various valves under consideration

2.6.1 Problem statement

Vosloo (2018) work showed great promise, hence the further work on this topic, with the focus on achieving a working configuration of a semi-active hydro-pneumatic suspension system that will allow continuous variable damping in a controllable manner. The system must be able to achieve the optimal spring and damper characteristics respectively for ride comfort and handling.

2.6.2 Research question

A new proposal for an architecture needs to be investigated to determine if it is feasible in achieving continuous variable damping in a controllable manner. The architecture need to be able to produce the optimal damping characteristic for both ride comfort and handling allowing for variability in between these two damping states. The architecture must also be modelled in a manner that will allow for full vehicle simulation i.e must be computationally efficient.

The proposed architecture, as presented in figure 2.16, will have a passive blow-off damper in parallel with the flow control valve. This is done to ensure controllability in the closed region of the variable valve. This damper will follow on the work of Els (2006) and Vosloo (2018). The selection of accumulators will be controlled by on/off solenoid valves giving independent control of the spring and damper characteristics. Hence it will allow for: at least 3 spring stiffness's (achieved with hydro-pneumatic springs), continuous variable damping (with the use of a flow control solenoid valve) and also incorporate a blow-off characteristic (blow-off valve is placed in parallel with the flow control valve).

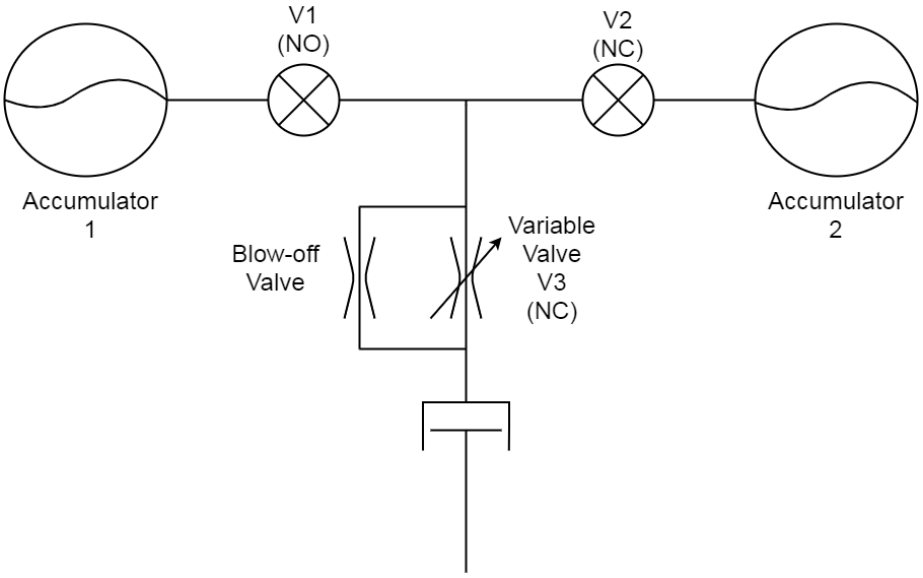

Figure 2.16. Proposed architecture for this study.

The proposed configuration consists of:

- **Gas accumulators:**

  As with the $4S_4$ & $4S_4CVD$ the configuration has 2 gas accumulators as developed and modelled by Els.

- **Hydraforce** $SV10-24/25$ **valves:**

  Valves 1 & 2 is the same valves as used in the $4S_4$. In this case the two valves are used in-line with each accumulator. These valve settings can be tailored to range from very soft to extremely hard by making use of the following selections:

  1. Valve 2 closed: accumulator 1 - spring characteristic 1.
  2. Valve 1 closed: accumulator 2 - spring characteristic 2.
  3. Both valve 1 and 2 open: accumulator 1 & 2 - soft spring characteristic.
  4. Both valves closed: compressibility of the oil - very stiff spring characteristic.

  The two valves are respectively a normally opened and normally closed valve. This will allow, in the event of power loss, for the system to revert to one of the intermediate spring setting for safety purposes.

- **Hydraforce** $ZL72-30$ **variable flow control valve:**

  The variable valve, V_3 depicted in figure 2.16 is the same flow control valve used by Vosloo (2018). This valve will be used to achieve variability in the damping of the set-up. The valve is a normally closed valve ensuring that in the event of power loss the suspension will revert to high damping for safety purposes.

- **Blow-off characteristic:**

  From the experimentally extracted damping data presented by Vosloo (2018). It is clear that the damping force, pressure drop over the valve, tends to infinity as the valve closes. Controlling the valve accurately in the vicinity of the fully closed position is challenging. This will require from the damper (shell, seals and valves) to withstand these high forces. This poses a problem and hence the need to limit the damping to a certain ceiling limit. The proportional valve is therefore placed in parallel with a passive blow-off damper valve that supplies the required high damping for optimal handling when the proportional valve is fully closed. Opening the proportional valve decreases the damping up to the point where the lowest damping is achieved with the proportional valve fully open. The high damping required for handling as set out by Thoresson (2007) is therefore provided by the passive blow-off valve with the low damping required for ride comfort, as well as the continuous variable damping, provided by the proportional valve.

The rest of the document will now describe the the experimental work, mathematical modelling and validation of the newly proposed suspension architecture.

3. Experimental Set-Up

In order to model and validate the newly proposed suspension architecture two experimental set-ups were developed. The first focused on characterisation of the blow-off valve and the second characterised the full suspension system. The experiments (addressed later in this chapter) shared similar hardware and data capturing requirements. This is by design to ensure that no unnecessary time is wasted in constructing numerous experimental set-ups.

3.1 Hardware

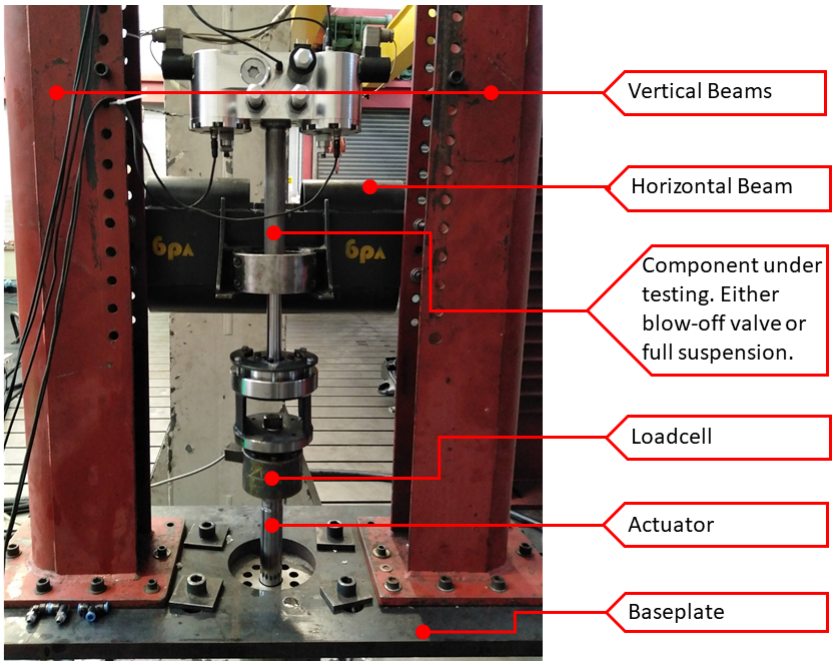

Figure 3.1. Mounting structure: H-frame used in performing the experiments.

The hardware used for mounting and actuating the test set-ups can be seen in figure 3.1. The actuation mechanism, a $25kN$ Schenck hydropulse actuator, was mounted on top of a vibration isolation test block. The support structure, H-frame, was fixed on top of the actuator. This allow for a rigid structure that will minimize structural deflection and vibration during testing. The test set-up can thus be mounted rigidly on the horizontal beam of the H-frame and the other end attached to the actuator via a load cell services (LCS) 5 Ton ULP load cell. It is assumed that structural deflection is minimal and as such the displacement of the actuator is equal to that of the strut used in the experiments. Spherical bearings ensure that slight misalignments will not induce external moments or additional forces on the test set-up other than the vertical force of the actuator.

Measurements during experiments were made with the following equipment:

- Suspension displacement: **Linear variable differential transformer (LVDT)** of the Schenck actuator was used.
- Suspension force: **Load cell**
- System Pressure: **50 MPa KYOWA PLG-A pressure transducers**.

3.2 Signal Conditioning and Data Capture

The experiments were aimed to easily extract the damping data in such a manner that adequate data for the other components is obtained simultaneously. This is best done with constant velocity signals. Therefore various constant velocity signals were created in Matlab. These digital signals were converted to analogue signals using a National modular signal generator. The analogue signal was then send to a Zwick $K7500$ servo controller, which require displacement and force feedback from the actuator's LVDT and the load cell to accurately control the Moog valves of the actuator. For the experiments the actuator was operated in displacement control seeing that the aim was to extract the corresponding forces for a specific velocity and displacement. A constant current signal was used in operating the continuous variable valve and switching the on/off valve. The current was manually tuned to a desired amperage using a GW-Instek $SPS-3610$ DC power supply.

During experiments up to seven channels needed to be sampled. These included:

- Displacement of the actuator.
- Force from the load cell.
- Up to 5 pressure readings from pressure sensors.

The displacement and force signals were sent through the National modular controller were the signals were amplified to an analogue range of $[-10V;10V]$ and filtered with a $400Hz$ low-pass filter before the signals were captured by a Diamond Systems Helios data acquisition module (DAQ) as can be seen in figure 3.2.
The pressure readings were amplified with an instrumentation amplifier ($AD8422$) with a low pass $LTC1563$ filter that has a cut-off frequency of $256Hz$ before it was sent to the DAQ.

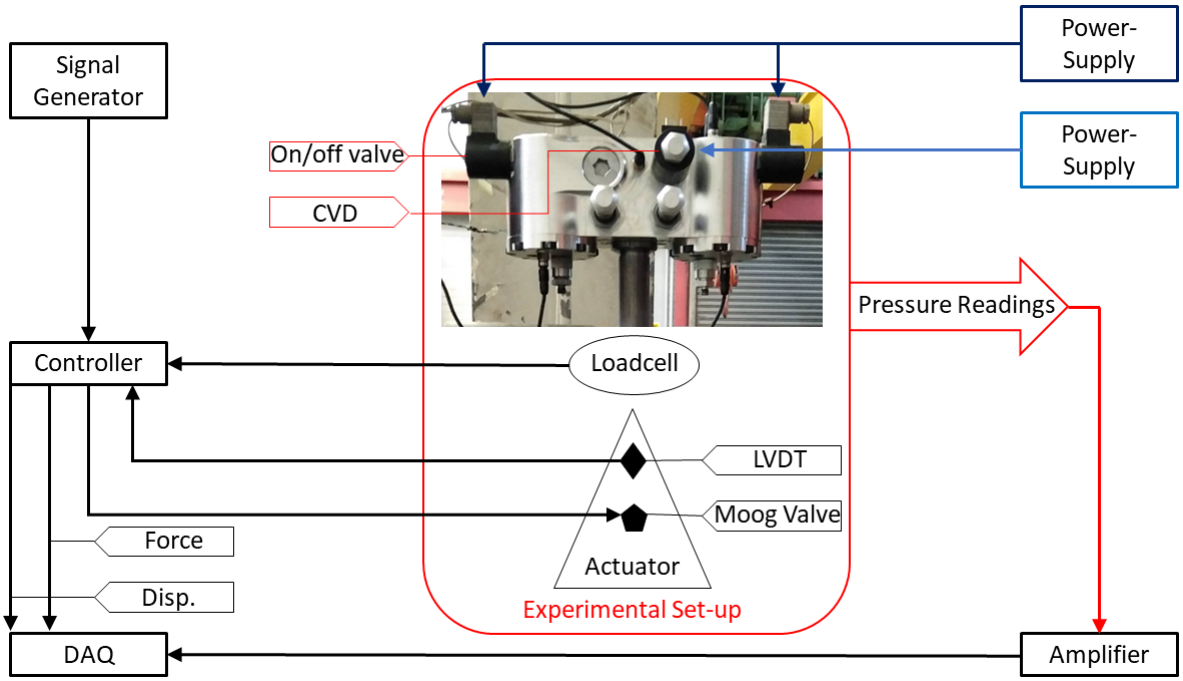

Figure 3.2. Schematic of the control and data capturing layout for the experimental set-ups.

Having the signals saved in a digital format it can be converted to the respective Engineering units using the relevant conversion factors.
All instrumentation were zeroed and calibrated before conducting experiments. Force and displacement limits on the actuator were set to ensure the safety of the test set-up.

3.3 Experimental Set-up 1: Experimental Blow-off Valve

Seeing that the blow-off damper was not included in previous hydro-pneumatic semi-active suspension systems considered in literature its functioning is uncertain. Therefore an experimental blow-off damper was designed and manufactured to investigate the functioning of a blow-off damper design and to validate a mathematical model against.

A blow-off damper, with adjustability in every stage, initial orifice area, knee point and total orifice area, is needed. The adjustability will allow for compensation towards the C_d value of the design. It will also allow the tuning of the damping force to a degree. Once an optimal/desired damping curve is achieved the blow-off damper, for actual application in the suspension system, can be manufactured and installed. This will ensure that the blow-off damper in the system will function as close as possible

to the optimal damping characteristic. The experimental blow-off damper will only allow for blow-off in one direction. It is assumed that the same behaviour in bi-directional flow can be achieved by duplicating the design in the opposite direction.

The assembly drawing of the experimental blow-off damper is included in Appendix A. Referring to the assembly drawing the following adjustments can be made:

1. **Stage 1:** The orifice area A_p can be adjusted using the needle valve.
2. **Stage 2:** The pre-load of the spring can be adjusted by screwing the shaft in or out.
3. **Stage 3:** The orifice area A_v can be adjusted by changing a grub screw that can have different orifice sizes.

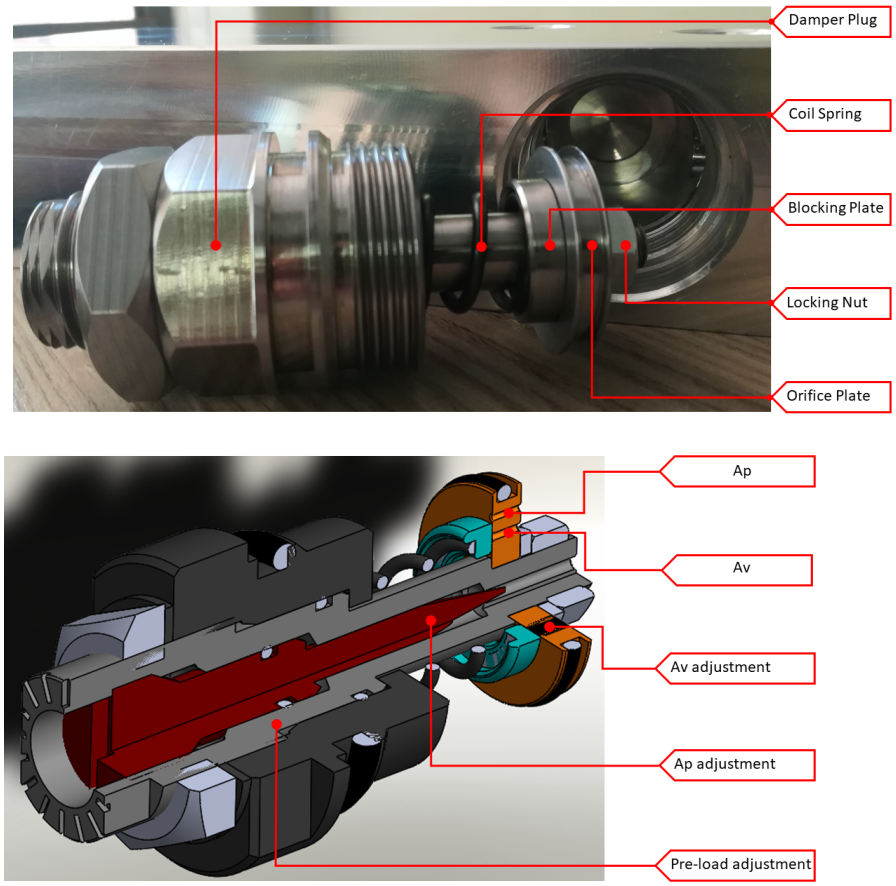

Figure 3.3. Manufactured blow-off experimental damper and testing block.

The valve block depicted in figure 3.4 mimics the entry and exit flow paths and cavity that the blow-off damper would have in the prototype design. This will ensure that minimal errors are made between the

experiment and the actual application. The blow-off valve is installed in a test block on the equipment set-up seen in figure 3.4. The test block allows pressure measurements just before and after the orifice plate. By inducing a known flow rate, knowing the orifice area and measuring the pressure drop over the valve, the C_d value can be obtained experimentally. The performance of the model can also then be compared with the experimental data.

The flow for this experiment was induced by a double acting cylinder (see figure 3.4) connected to the actuator via a rose joint. Due to the larger piston size of the double acting cylinder the induced flow rate for a certain velocity is higher than it would be for a $32mm$ diameter piston used in the prototype design. This was compensated for by actuating the cylinder at a lower velocity making use of the relation:

$$v_{DaC} \cdot A_{DaC} = v_{proto} \cdot A_{proto} \tag{3.1}$$

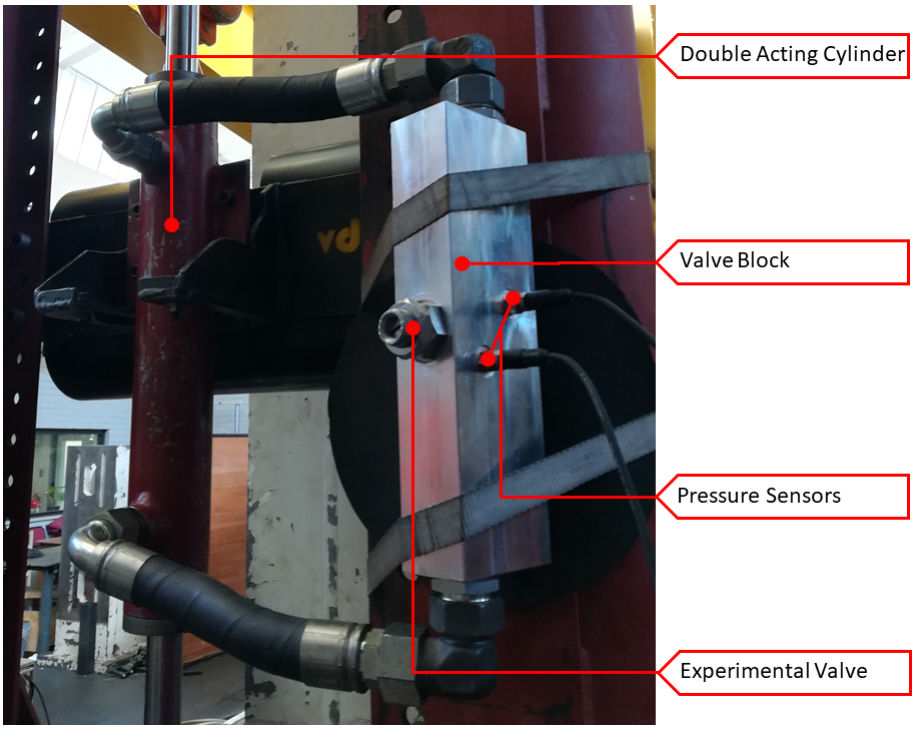

Figure 3.4. Experimental blow-off damper and block test set-up.

An iterative experimental process was followed to ensure that the damping characteristic will be as close as possible to the optimal/desired damping curve. By making adjustments to all the aspects of the experimental valve as the capability allows for. The stage 1 damping curve and the blow-off point could be matched close to the optimal/desired curve. Once this point was reached the entire damping envelope could be extracted and hence the working principal of the experimental blow-off valve.

Measuring the displacement of the actuator and the pressure readings from the pressure sensors it is possible to obtain the force-velocity characteristic of the experimental blow-off damper by:

1. Numerically differentiating the displacement from the actuator to obtain the velocity.
2. Determining the region of constant velocity.
3. Averaging the pressure readings for the constant velocity regions.
4. The force that the damper produces for a certain velocity can be determined by:

$$F = (P_2 - P_1) \cdot A_{piston} \tag{3.2}$$

   This produces one data point on the graph of force vs. velocity for the experimental damper.
5. Repeat steps $1-4$ for every velocity considered in the experiment.

3.3.1 Spring characterization

Experiments were conducted to determine the spring characteristic of the spring that was used in the experimental blow-off damper, the model and ultimately in the prototype.

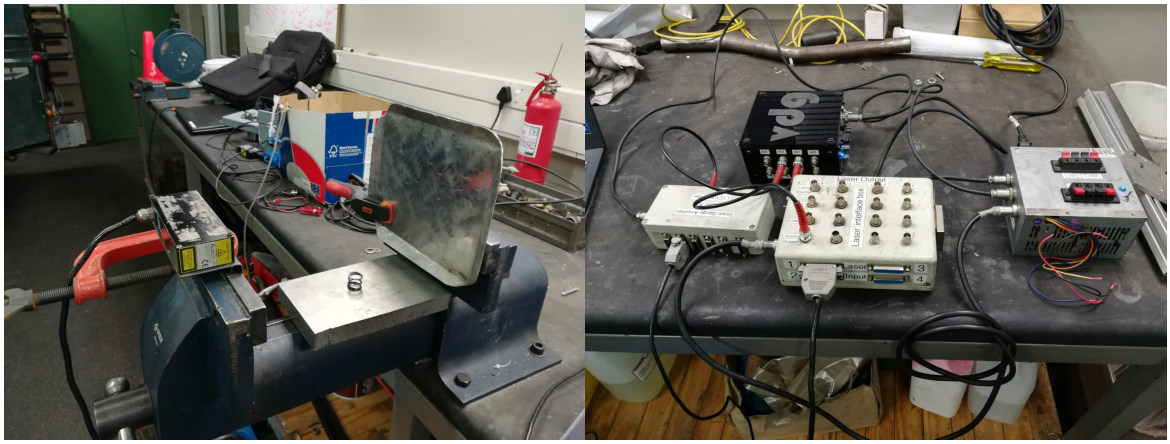

Figure 3.5. Spring characterization experiment.

The equipment used, (Acuity Laser displacement Sensor AR-700-8RP) and 50kg S-type load cell, were calibrated in the expected operating region. The spring was compressed with multiple increments throughout its working range. While the spring was compressed, the displacement and force was recorded. The load cell measurement was amplified before being sampled by the DAQ.

The data was processed and plotted on a graph of force *vs* displacement, as the gradient of this line represents the spring stiffness. A Bayesian model was used to fit a line through the data. The Bayesian model was used because the regression could be weighted more towards either the data or the proposed

model. Seeing that this is a linear spring, the weighting was set to be more towards the model than the data. The experimental data and regression are presented in figure 3.6.

From figure 3.6, it is clear that the experimental data has a very strong linear trend as expected. Although the Bayesian model is shifted below $0N$ the model fits the data reasonably well. The shifted off-set may be due to the fact that the model includes a y-intercept. However, the gradient of the line and hence the spring stiffness of the spring was determined to be $21.99N/mm$

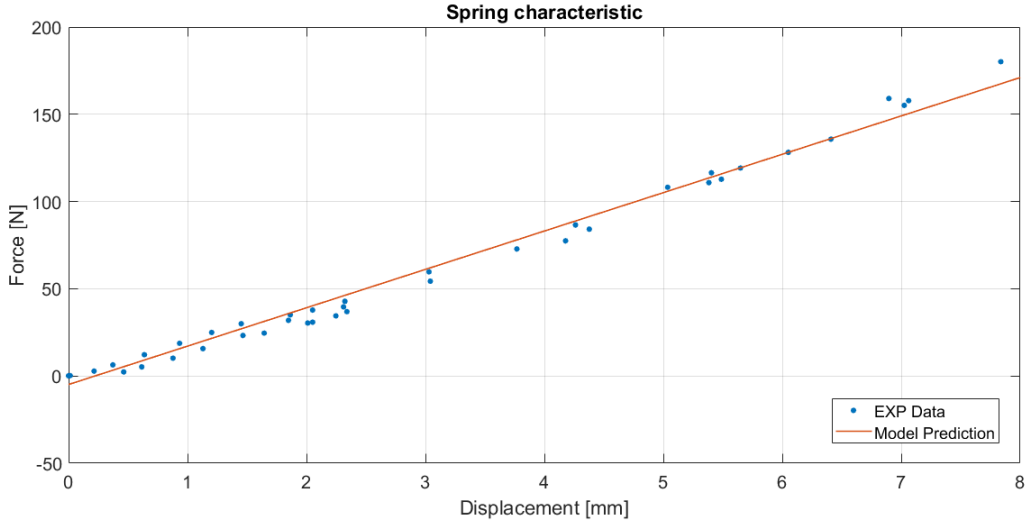

Figure 3.6. Experimental results for determining the spring stiffness the spring for the blow-off damper model.

3.4 Experimental Set-up 2: Full Prototype Testing

To determine if the proposed architecture is feasible a full prototype needed to be developed for experimental testing. The design included known mechanisms that proved good functionality in literature (e.g. hydro-pneumatic accumulators and $SV10-24$ valves) as well as a bi-directional blow-off damper based on the knowledge gained from experiment 1. The initial design is presented in figure 3.7.

During the experimental stage numerous design flaws and errors arose. These flaws led to design changes that altered the initial design presented in figure 3.7.

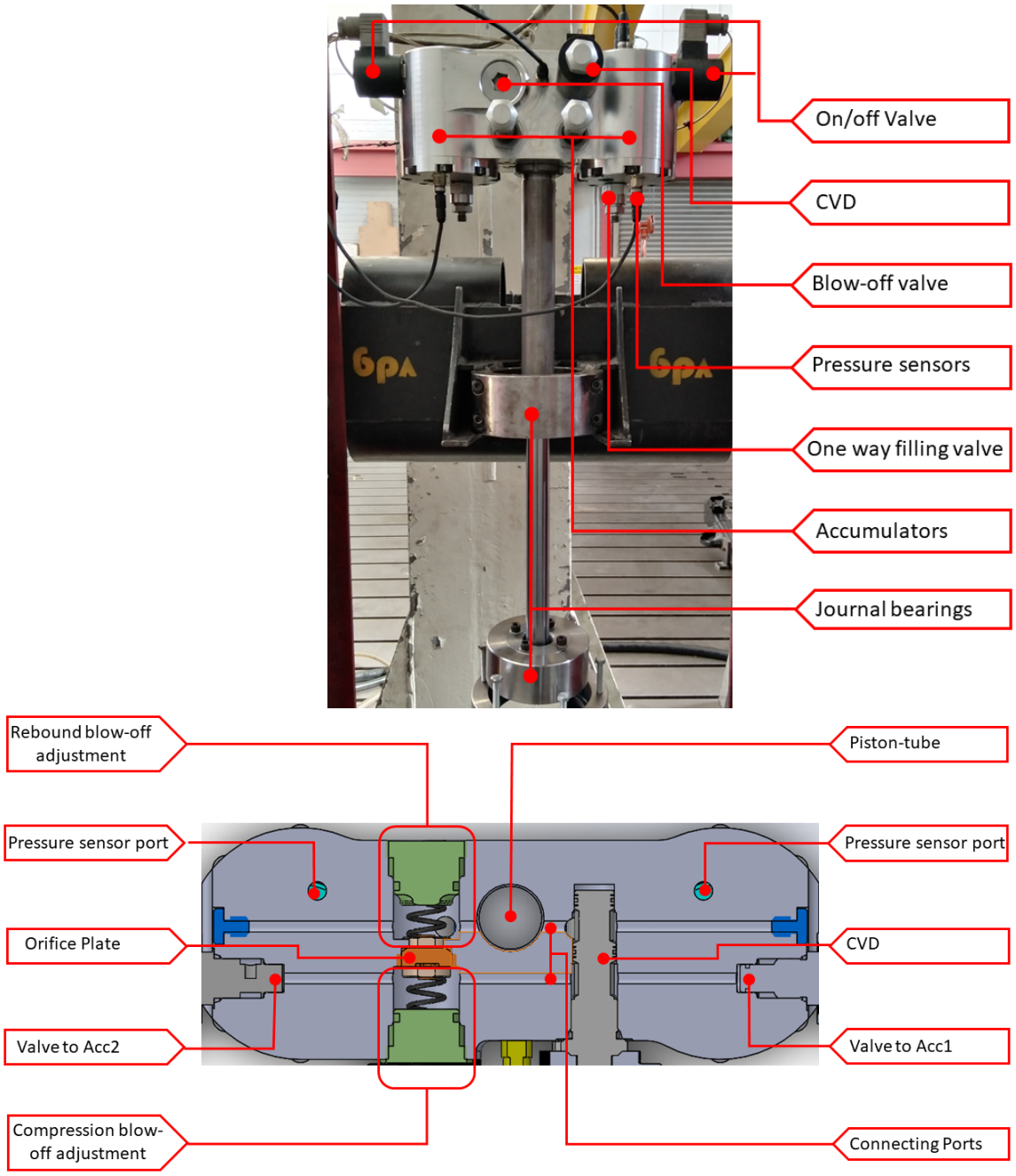

Figure 3.7. Initial prototype and bi-directional valve in parallel with the continuous variable valve.

The biggest design change that had to be implemented is the change back to floating pistons for the gas accumulators. In an attempt to reduce the friction, Vosloo (2018) replaced the original floating pistons accumulators with rolling diaphragms. The diaphragms tore repeatedly during testing and after trying to solve the problem it still persisted. The original floating piston accumulators were installed to enable testing. Els (2006) optimized the accumulator sizes of the $4S_4$ for optimal ride comfort and handling. Seeing that the prototype has a smaller piston diameter the floating piston accumulator sizes has to

account for this. The two accumulators for the prototype thus have a $0.16l$ accumulator (equivalent to the $4S_4$'s $0.4l$ accumulator) and a $0.04l$ accumulator (equivalent to the $4S_4$'s $0.1l$ accumulator). The spring characteristics remain unchanged. The change in accumulators can be seen in figure 3.8

Figure 3.8. Prototype iteration including floating pistons.

3.4.1 Gas charging procedure

To ensure that there is no air trapped in the oil and that the gas accumulators have the correct static pressure at the correct gas volume the following procedure needs to be followed when filling the unit with oil and charging the accumulators with gas. Strict adherence to this procedure is required to ensure initial conditions are known with the least uncertainty:

1. Ensure the the piston is at the top of its available travel.
2. Create a vacuum ($150 - 200mbar$) at the gas side of the floating piston to ensure that the floating pistons is at the bottom of the accumulator. As an additional precaution the gas bleeding bolt can be removed to measure the distance from the end cap to the bottom of the floating piston (it should be 25 mm) with a Vernier. Ensure that the vacuum is collapsed before removing the bolt. This vacuum needs to be maintained during the oil filling process to ensure the piston remains at the bottom.

3. The unit will be filled with oil making use of a vacuum. This will require an oil bath with a valve connected at the inlet port of the suspension unit (in this case the pressure sensor port on the top of the $0.16l$ gas accumulator). The outlet port (pressure sensor port on the top of the $0.04l$ gas accumulator) needs to be connected to the vacuum pump also isolated with a valve. For an illustration refer to figure 3.9. To fill the unit with oil:

   (a) Ensure that both the $SV10-24$ valves are open and that the two in-line valves are closed.

   (b) Create a vacuum by operating the vacuum pump.

   (c) Open the in-line valve on the vacuum side to draw air out of the unit. After a few seconds close the valve.

   (d) Open the in-line valve on the oil side and keep it open until the oil level in the oil bath stops changing. Then close the valve again.

   (e) Repeat steps c & d until the oil entering the vacuum chamber does not contain any more air bubbles.

4. After the unit is filled with oil the vacuum can be collapsed, the equipment removed, the pressure sensors installed and the $SV10-24$ valves closed. The unit is now filled with oil and the gas can be charged in the accumulators.

5. To ensure that the floating piston will push the oil as the piston is moved downward, charge the $0.04l$ accumulator with $1.5MPa$ of Nitrogen gas (referred to as the preliminary charge) in the current position. Open the $SV10-24$ valve for the $0.04l$ accumulator.

6. Once the $0.04l$ accumulator is preliminary charged move the piston down by $34.31mm$. This will ensure that the gas volume is $0.04l$. The accumulator can now be charged to $6.5MPa$. This will ensure a static force of $5kN$. Close the $SV10-24$ valve for the $0.04l$ accumulator.

7. Open the $SV10-24$ valve for the $0.16l$ accumulator. Once the $0.16l$ accumulator is preliminary charged move the piston down by $137.27mm$. This will ensure that the gas volume is $0.16l$. The accumulator can now be charged to $6.5MPa$. This will ensure a static force of $5kN$. Close the $SV10-24$ valve for the $0.16l$ accumulator.

8. The static position of the strut can now be adjusted by adding or draining oil with both $SV10-24$ valves closed. This step requires high pressure valves as well as an auxiliary power unit. This was not considered in the experiments but the prototype makes provision for it with the use of 2 additional proportional flow control valves.

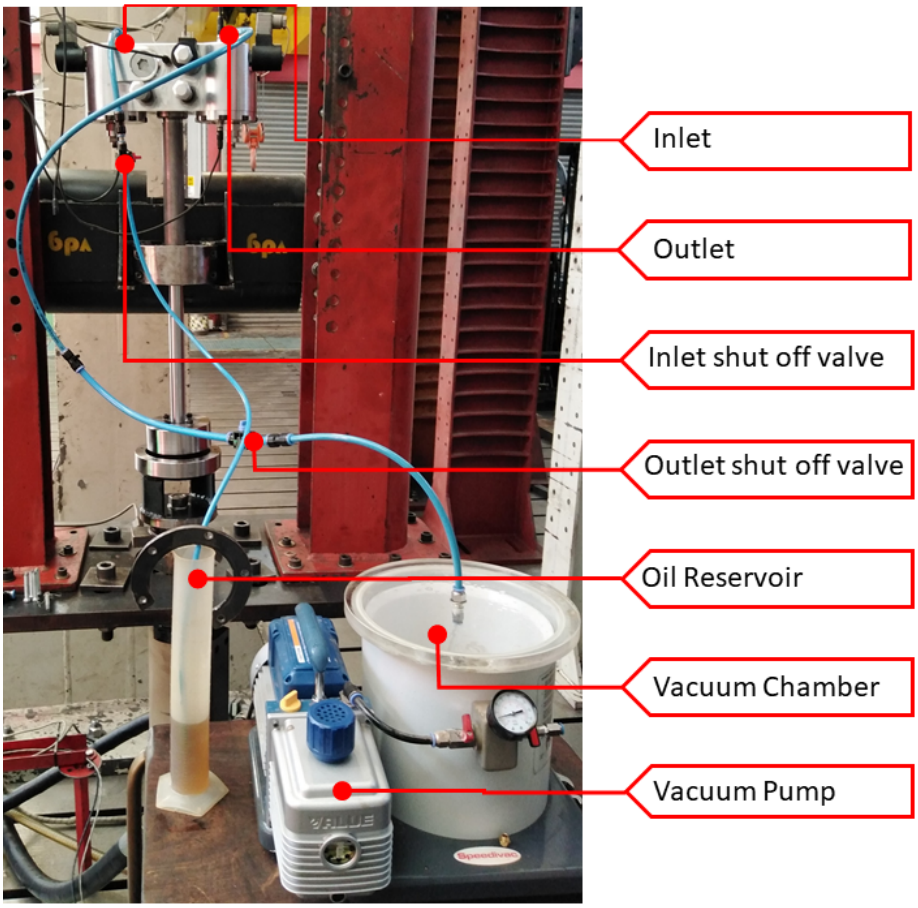

Figure 3.9. Illustration of set-up for filling the unit with oil using a vacuum.

The data collected during testing using the experimental set-ups can now be used for parametrising and validating the model that will be developed in chapter 4.

4. Mathematical Modelling

A mathematical model of the semi-active suspension system is required that can calculate the force produced as a function of the suspension displacements and velocity, as well as other considerations such as the ambient temperature and switching signals to the valves. The system model has to include the following:

- Accumulator gas models.
- Flow control valve characteristic.
- Blow-off valve characteristic.
- Friction of the system.
- Response times of the valves.
- Oil compressibility.

Some of the components in the proposed configuration as in figure 2.16 were previously modelled and tested in experiments as presented in literature. Although this was done for different configurations of the original $4S_4$ it is assumed that the individual components differ insignificantly compared to previous versions. The differences are on the configuration of the components and not their functioning. The modelling of these components from literature can thus be employed in this section.

4.1 Damper Model

4.1.1 Basic valve model

To understand the basic working and mathematics behind the combination of orifices and mechanical components, Dixon (2007) presents a simple model as depicted in figure 4.1(a). The resultant $P(Q)$ curve is presented in figure 4.1(b).
This simplified model consists of 2 orifice areas in parallel, with one of them being a variable opening area (A_v, for this model, consider linear opening). This will result in 3 stages as set out in figure 4.1(b):

- **Stage 1:** This stage determines the flow with the variable valve A_v being fully closed.
- **Stage 2:** This stage is the transition from the valve being fully closed to the valve being fully opened. The dimensionality of the transition is determined by the mechanism being used (or modelled) to achieve the valve opening.
- **Stage 3:** Once the valve is fully open the orifice area is equal to the 2 orifices being in parallel, and the normal flow equations can be used to determine the flow through the orifices.

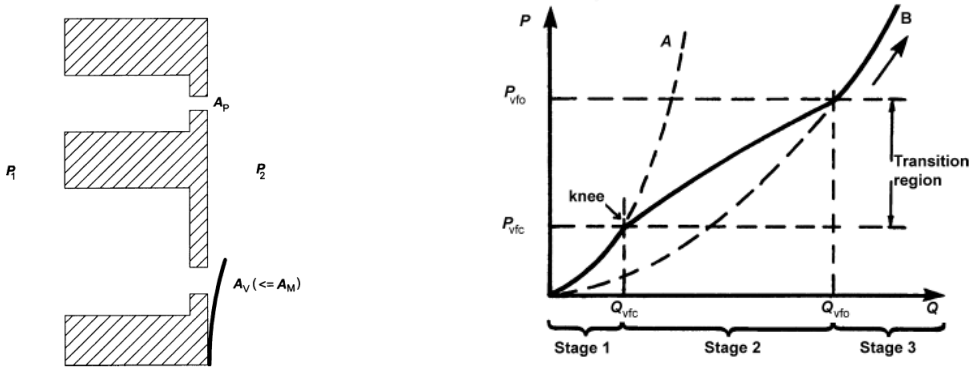

(a) Basic valve model. **(b)** Characteristic of the valve and the transition.

Figure 4.1. Basic valve model and characteristic considering the combination of orifice flow and compliant members. (Dixon 2007)

Considering the equations and relations for orifice flow as presented in section 2.3 this basic model can be described mathematically as follows:

$$\left.\begin{array}{ll} Q = A_p\sqrt{\frac{2\Delta P}{\rho}} & P \leq P_{vfc} \\ Q = \left\{A_p + \left(\frac{P-P_{vfc}}{P_{vfo}-P_{vfc}}\right)A_m\right\}\sqrt{\frac{2\Delta P}{\rho}} & P_{vfc} < P < P_{vfo} \\ Q = \{A_p + A_m\}\sqrt{\frac{2\Delta P}{\rho}} & P \geq P_{vfo} \end{array}\right\} \tag{4.1}$$

The proposed configuration incorporates a blow-off valve in parallel to the flow controlled solenoid valve (continuous variable damping will be achieved with this valve). This blow-off valve is a passive damper that can be modelled with the basic valve model. The orifice area A_p will be used to achieve the optimal handling characteristic presented by Thoresson (2007) and the orifice area A_v will be designed so that the transition stage will be over a wide range of the expected flow rates that the damper will experience in operation. By using the parallel valve configuration, it is possible to create an upper ceiling for the pressure and ultimately limiting the damping force in the region where the proportional valve is nearing the closed position.

4.1.2 Damping variability

The flow through the flow control valve can be described mathematically with the volumetric flow equation set out by Dixon (2007):

$$Q_{CVD} = A_p\sqrt{\frac{2\Delta P}{\rho}} \tag{4.2}$$

However the area given by A_p varies according to the input current supplied to the solenoid. A relation needs be obtained between the opening of the valve and the current supplied. To determine this relation, the experimental damping data Vosloo (2018) extracted for the flow control solenoid valve, presented in figure 4.2, is used to build this relation using equation 4.2. The equivalent $C_d \times A$ of the orifice can be approximated for the different supply currents considered in this data.

Also presented in this figure is the pressure drop over the valve, when employing equation 4.2 with the calculated areas. It is clear that a small error is made in this approximation. However, the model can later be adapted to fit the experimental data for the proposed configuration.

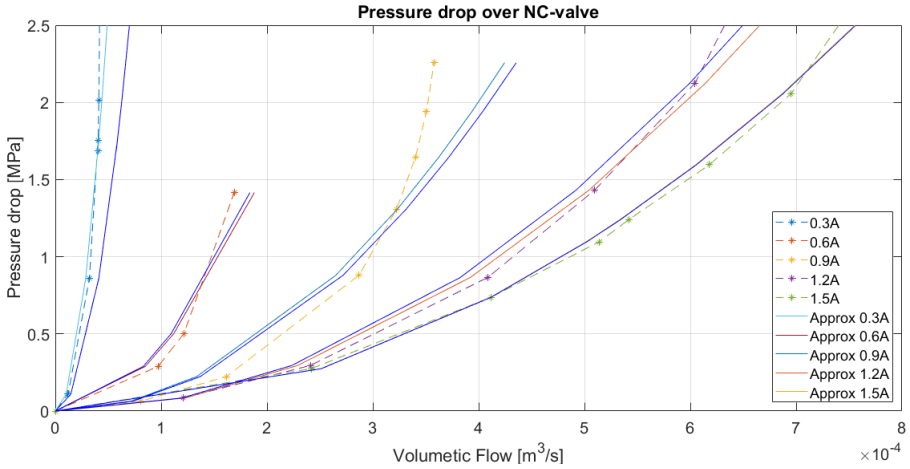

Figure 4.2. Determining the orifice area of the flow controlled solenoid valve.

The areas calculated above is now plotted against the supply currents to the valve, as presented in figure 4.3. This plot shows the relation as expected. When the valve is fully closed, the area should be zero. The area should increase from this point to a maximum value that is related to the valve being fully open.

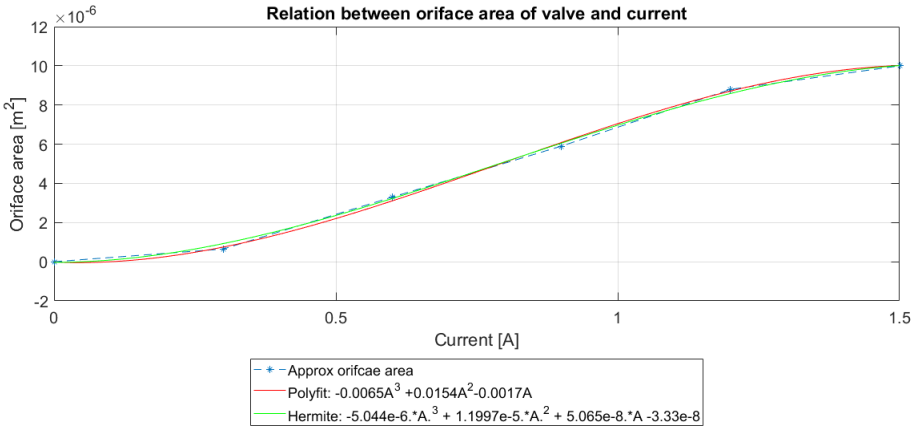

Figure 4.3. Fitted hermite polynomial through the orifice area *vs* supply current.

To determine the orifice area for any supply current ranging from $0A$-$1.5A$ a 3^{rd}-order Hermite polynomial is used to model the relation between the supply current and the orifice area

$$Area = -5.044e^{-6}Current^3 + 1.1997e^{-5}Current^2 + 5.065e^{-8}current - 3.33e^{-8} \quad (4.3)$$

This is done under the assumption that the increase in area between the experimental points follow the trend depicted in figure 4.3. A Hermite polynomial is used because of the better control that can be applied to the gradient at the upper and lower ends of the polynomial. This is done to represent the physics better i.e to ensure that no negative areas are obtained and that the maximum area never exceeds the biggest calculated orifice area. The polynomial fit is presented in figure 4.3. Also shown is a regular 3^{rd}-order polynomial fit using the $polyfit$ function in Matlab. This is presented to show the misrepresentation that is improved by using the Hermite polynomial.

The pressure drop over the variable damper for a certain supply current to the solenoid can now be determined. Seeing that this orifice is modelled to be in parallel to the blow-off orifice, the flow rate through this orifice can be added to the blow-off orifice flow rate as indicated in equation 2.3 to determined the damping force.

4.1.3 Blow-off damping model

In order to use the basic valve model it is required to determine the parallel and total orifice areas, as well as the pressures at which the valve will be fully closed and open.

To determine the orifice areas A_p & A_m in equation 4.1 the optimal damping characteristic for handling is considered as depicted in figure 2.3. Following the same process as with the variable valve as described in section 4.1.2 these areas were determined to be $1.2mm^2$ & $3mm^2$ respectively.

The pressure at which the valve is fully closed and fully open is determined by the mechanism used to achieve the blow-off. In this case, a linear coil spring (with a spring stiffness of $21.99\frac{N}{mm}$) as determined in section 3.3.1) is used to achieve this. The P_{vfc} can be calculated as follows:

$$P_{vfc} = \frac{K \times Preload_{spring}}{A_m} \quad (4.4)$$

The pressure at which this valve is fully open is the crossing point between the pressure drop caused by the orifice with area A_m and the transition line as presented by figure 4.1(b). This pressure will be due to the geometry of the blow-off valve opening mechanism. The moment when the opening is bigger

than the orifice area A_m the valve is fully open, and this pressure can be determined as follows:

$$P_{vfo} = \frac{K(Preload_{spring} + Displacement_{fullyopen})}{A_m} \tag{4.5}$$

with $Displacement_{fullyopen}$ referring to the opening mechanism's induced annular area being bigger than the orifice area A_m. For this model $Displacement_{fullyopen} = 0.1mm$ due to the fact that the blow-off valve model represents the physical manufactured experimental blow-off damper used in experiment 1 as in section 3.3

All the information needed to compute equation 4.1 is acquired. However, if one considers the equation for the transition zone:

$$Q = \left\{ A_p + \left(\frac{P - P_{vfc}}{P_{vfo} - P_{vfc}} \right) A_m \right\} \sqrt{\frac{2\Delta P}{\rho}} \tag{4.6}$$

It is clear that there is a non-linear relation for the pressure that features in the fraction of the valve opening as well as the pressure drop over the valve. In order to solve the pressure drop over the valve for a certain flow rate induced by the piston in this area, a numerical method must be used to determine the pressure drop. The Secant method is used for this computation as it does not require a derivative which reduces computational demand while still providing a good convergences rate.

The output of the model is presented in figure 4.4. Also presented is the optimal damping characteristic for the compression of the damper. For the time being the damper characteristic for compression is mirrored for rebound. From this figure, it is clear that the initial region of the blow-off damper mimics the optimal characteristic very well. However, the transition stage deviates significantly from the optimal characteristic. This is mostly attributed to the spring stiffness of the spring used as the blow-off mechanism. This spring does create a ceiling for the damping force, which is so by design. However, more work is needed to shift this ceiling towards the optimal curve. Another problem that might occur with this set-up is damper flutter in the transition stage. Seeing that the difference in force from the start of the blow-off to the start of stage 3 is so small, any deviation from this force band ($3550N - 3640N$) will cause the blow-off valve to open and close uncontrollably. This is known as damper flutter. This is mainly due to the spring stiffness of the blow-off mechanism being too low.

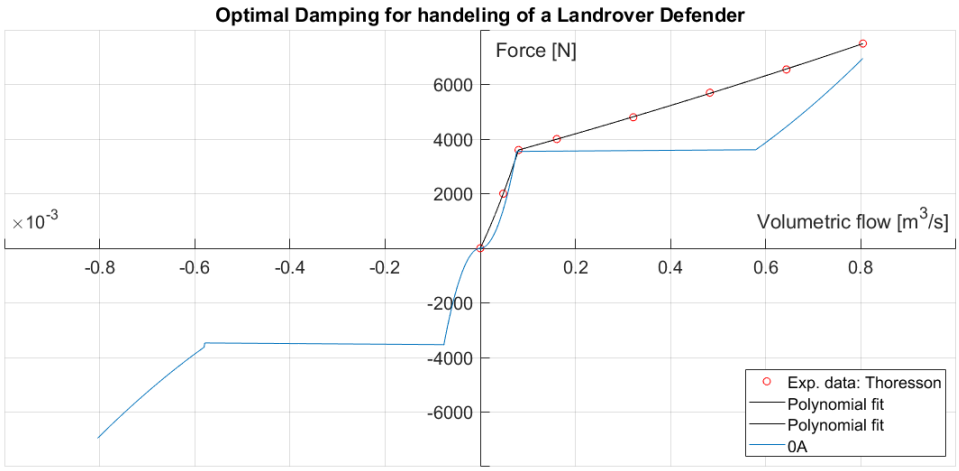

Figure 4.4. Output for the blow-off damper model.

4.1.4 Experimental blow-off damper

The design of the experimental blow-off damper presented in section 3.3 was based on the knowledge gained from the blow-off damping model. The experimental damper was manufactured to validate the blow-off damper model and to test its functionality. The experimental data obtained from experimental set-up 1 using the test procedure described in section 3.3 is presented in figure 4.5.

From this figure it is clear that the basic working principal of the experimental blow-off valve is as expected. Stage 1 & 2 is clearly visible as well as the transition between the 2 stages. Note that there seems to be some transients occurring at the transition/blow-off point (seen by the 2 ”outlier” data points). Also note that the transition stage is not a linear line. As for the functionality of the design for the blow-off damper it is clear that the working principles is as expected and that the design might be adequate in performance for a full prototype application.

Figure 4.5 depicts the damping model output making use of the physical parameters of the experimental set-up ($C_d = 0.65$ as obtained from the experimental data). It is clear from the figure that the model can predict stage 1 accurately and that some work is needed in stage 2. It should be noted that iterations on the pre-load of the spring for the blow-off point and the duration of opening for the blow-off valve was needed to obtain the fit as presented. This emphasises the need for improved modelling in the transition region.

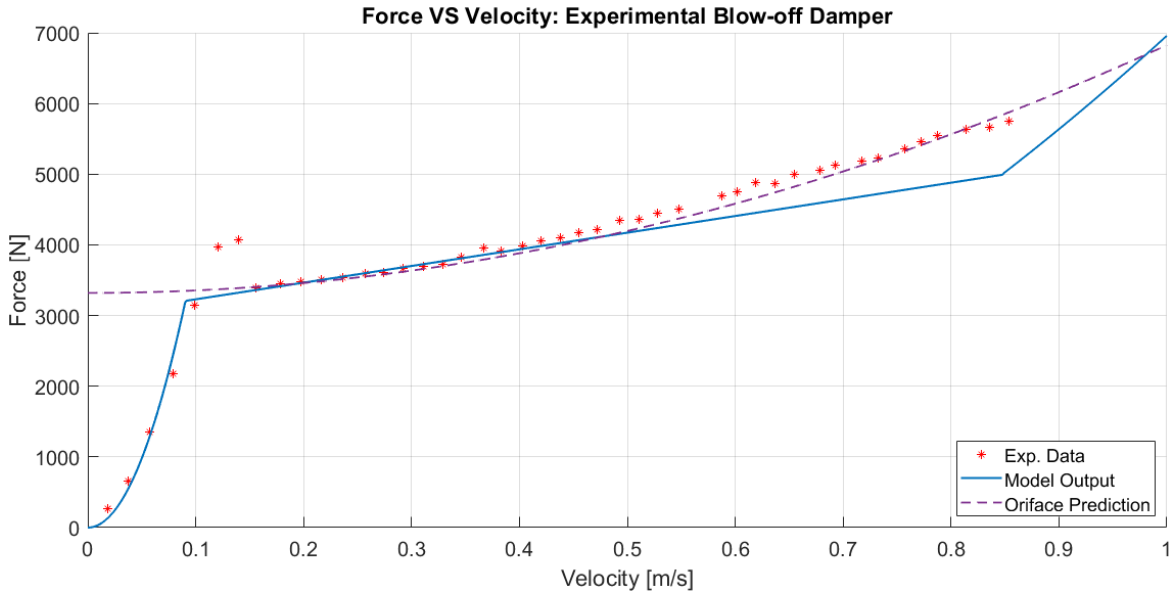

Figure 4.5. Comparison between the blow-off damper model and experimental data.

In order to relate the flow of stage 2 with a physical phenomenon the orifice flow equation 4.2 was employed. From figure 4.5 it is clear that by using equation 4.2 the transition stage can be closely related to the flow through an orifice. This excellent correlation gives an indication that the transition stage is clearly not a function of the blow-off mechanism (in this case the linear spring loaded valve). The transition stage is rather a function of the flow through an equivalent orifice causing a corresponding pressure drop.

The orifice area prediction can be related to an annular gap between the orifice and blocking plates. Hence the mechanism used in the blow-off valve may be linear but the flow is dominated by the quadratic function of the oil flowing through the annular area. The quadratic effect might also be due to orifices in series as presented by Dixon (2007) in figure 2.12. From this figure it is also evident that the series orifice area needs to be smaller than the blow-off orifice in order to have the quadratic effect. This is not the case in the experimental blow-off valve design.

To account for the discharge coefficient obtained in the experiment, the effect of the different orifices in the blow-off damper is presented in figure 4.6. From figure 4.6 it is clear that the pressure drop over the annular area of the blow-off valve will always be greater than that of the orifice area A_m.
Thus the dominating pressure drop will always be caused by the annular area around the blocking plate with this configuration of orifices.

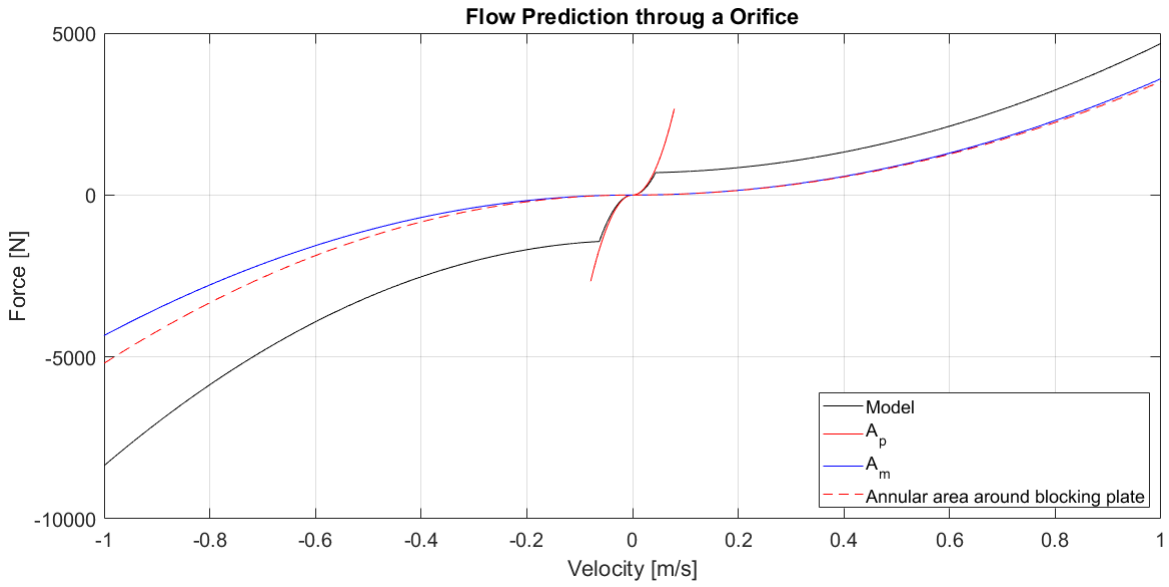

Figure 4.6. Governing area for flow in the transition region.

From the experiment it is evident that the damping model originally employed in modelling the damping of the experimental blow-off valve is not adequate and requires improvement.

The original idea of using the basic valve model as presented by Dixon (2007) can still be used with the following adaptions:

- A_v as presented in figure 4.1 is modelled as the annular area around the blocking plate respectively for compression and rebound damping.
- Seeing that the blocking plate needs to move only a fraction (approx. $0.2mm$) there is no transition stage and the blow-off characteristic has an on/off nature.

4.1.5 Damping characteristics of prototype

The design and development of the prototype used in experimental set-up 2, as described in section 3.4, relied on the knowledge gained from the preliminary experiments performed with the experimental blow-off valve.

The functionality and result, extracted from the data obtained with experimental set-up 2, of the proposed damping architecture (blow-off valve in parallel with the proportional flow control valve) is presented in figure 4.7. This figure also shows the damping envelope that can be achieved. It is clear that the blow-off valve was successfully duplicated in both the flow directions allowing for

a difference in the knee point and transition damping curve for both the rebound and compression damping separately.

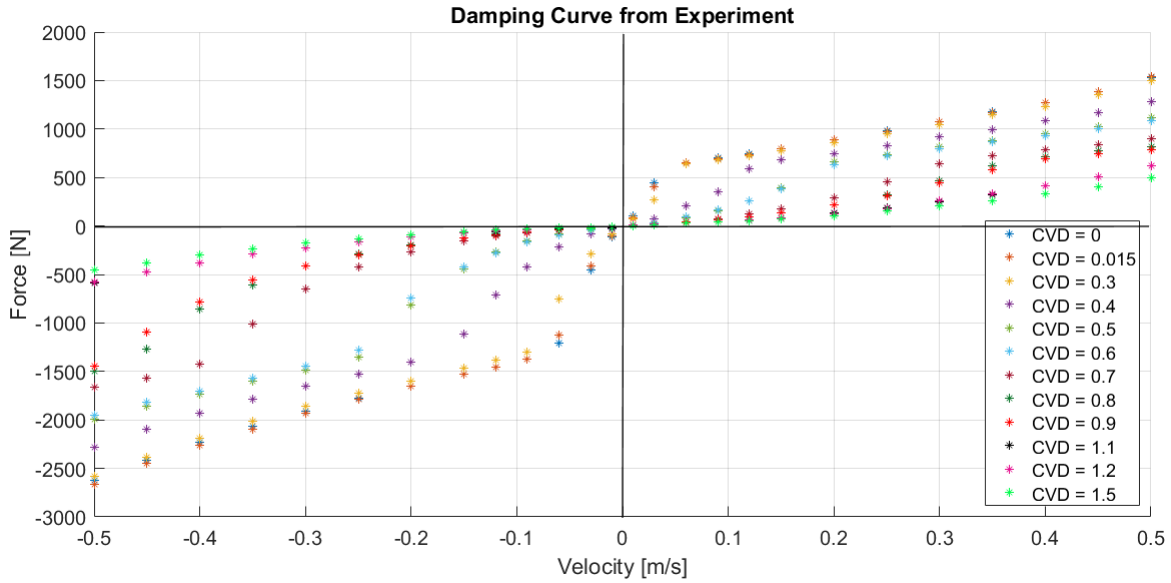

Figure 4.7. Full damping envelope of prototype considered during experimental testing.

4.1.5.1 Continuous variable damping

The blow-off damper was place in parallel with the continuous variable valve to allow for variability from very low damping up to the point of an optimal/desired damping curve. From figure 4.7 it is clear that the operation of the first stage is as expected. With extremely low damping while operating the valve in the fully open region and the damping curve emerging to the damping characteristic of the blow-off valve as the CV-valve is gradually closed. This then ensures that in the high non linear region of the CV-valve the system is protected from large pressure differentials while still maintaining adequate damping.

Note that the region of operation for the CV-valve, that will ensure a noticeable difference in damping, is in the middle ($0.3A$ - $1A$) of the valve's capable range ($0A$ - $1.5A$). Although the CV-valve setting has the lowest damping curve for $1.5A$ and the highest damping curve for $0A$. Operating the valve close to these regions results only in small changes to the damping curve, due to the non-linearity of the valve. The region for active controllability will be advised to be in the $0.3A$ - $1A$ range while using the fully open and fully closed setting for the extreme cases of handling and ride comfort.

4.1.5.2 Blow-off

From the experiment it is clear that the blow-off point occurs consistently at a constant force. These forces are presented in figure 4.8 for both compression and rebound. From this figure it is clear

that if the damping force from stage 1 reach the blow-off force a transition in the damping curve occurs.

The blow-off characteristic of the system functions as intended by providing a force ceiling and constant point of transition to a lower damping characteristic. Adjustability in the blow-off force can be achieved by changing the pre-load on the spring for both compression and rebound damping respectively.

The blow-off point is significantly lower than expected for the pre-load used in the experiment based on the modelling of the blow-off point as with equation 4.4. It is therefore clear that the opening of the blow-off valve is more complex than anticipated. Figure 4.9 shows fluctuations in the strut pressure in the region of the blow-off point. These fluctuations were anticipated seeing that a linear spring was used in the blow-off mechanism. Notice the sharp peaks when blow-off begins this also indicates that the flow opening the blow-off valve cannot be modelled with simple force - pressure relation acting on an area.

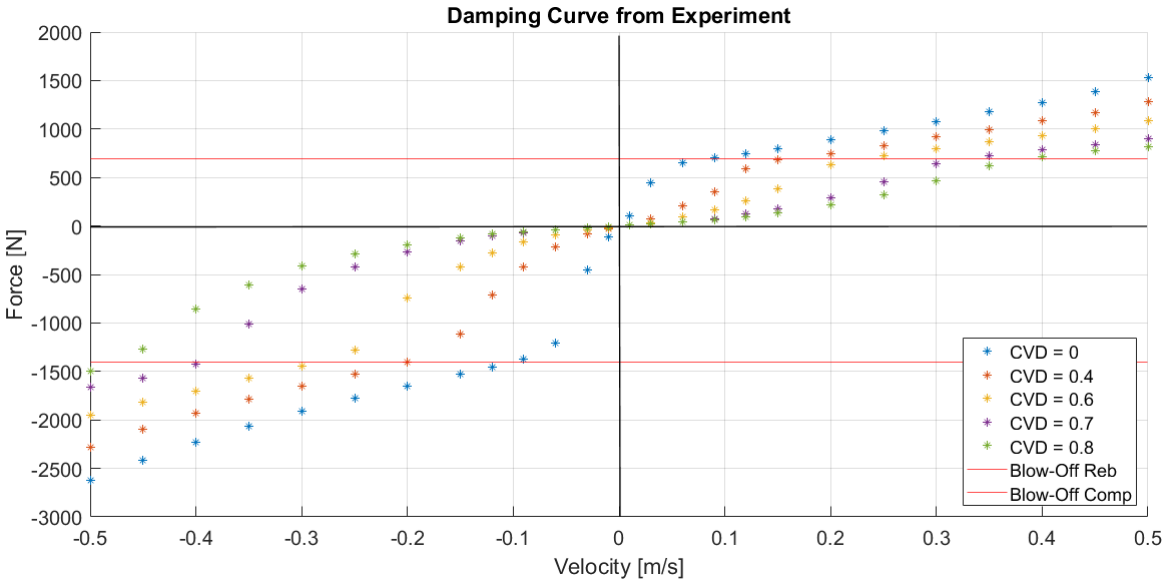

Figure 4.8. Blow-off points of the prototype.

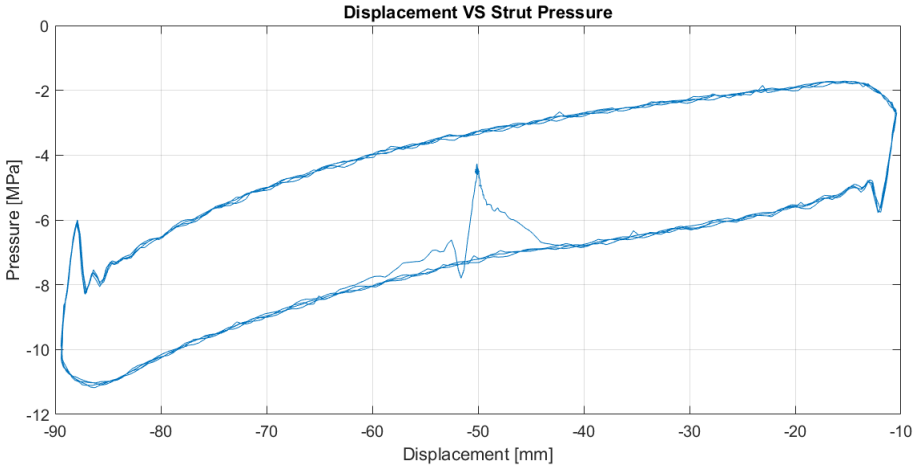

Figure 4.9. Fluctuation in the damping characteristic in the region of the blow-off point.

4.1.5.3 Transition damping stage

It was presented that the quadratic curve appearing in the transition region of the damping curve is due to flow through an orifice rather than being governed by the opening of the blow-off mechanism. From figure 4.10 it is clear that the same curve can be fitted to the experimental data once blow-off is reached for any setting of the CVV. A horizontal shift of this curve can be seen with the changing in the CVV setting. This shift is due to the fact that flow trough the blow-off orifice area is zero until blow-off occurs, where-after flow through this region increases with an increase in strut velocity.

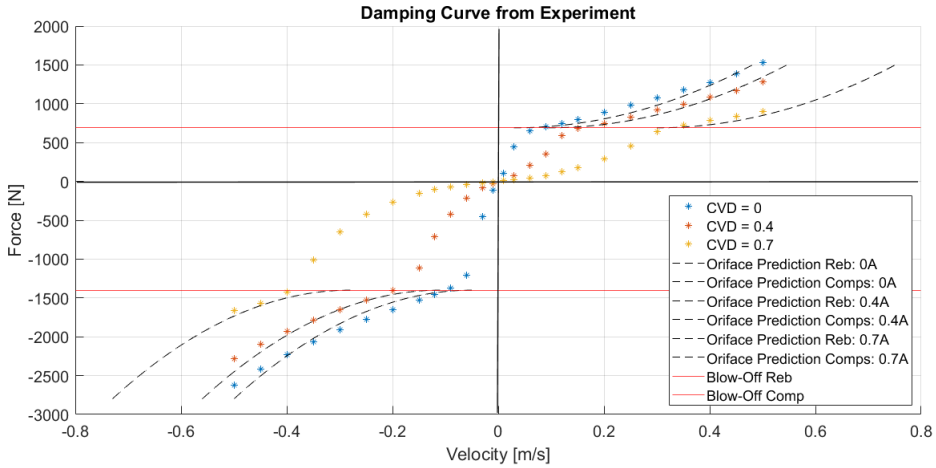

Figure 4.10. Transition region flow area investigation.

The orifice area predictions as presented in figure 4.10 is related to the annular gap between the orifice and blocking plates as expected from the experimental damper experiment and discussion of section 4.1.4.

4.2 Friction Model

The friction force is very low compared to the spring and damper forces it should therefore be noted that the uncertainty of the data presented in this section is high, seeing that very low forces (20N-200N) is extracted from a 50kN load cell. Thus the extracted data is expected to be in the noise-band of experimental set-up 2 as presented in section 3.4 and will show some fluctuation/variation.

The operating pressure of a hydraulic system is expected to have a large influence on the friction profile. It is expected that with higher pressures the friction will increase seeing that the seals is under higher hydraulic pre-loading. Hence the friction profile of the prototype is extracted at the operating pressure expected for vehicle implementation.

The force exerted by the whole unit is measured using a load cell. The measured oil pressure in the strut is converted to force using the piston area. The friction profile can be calculated as the difference between the two forces.

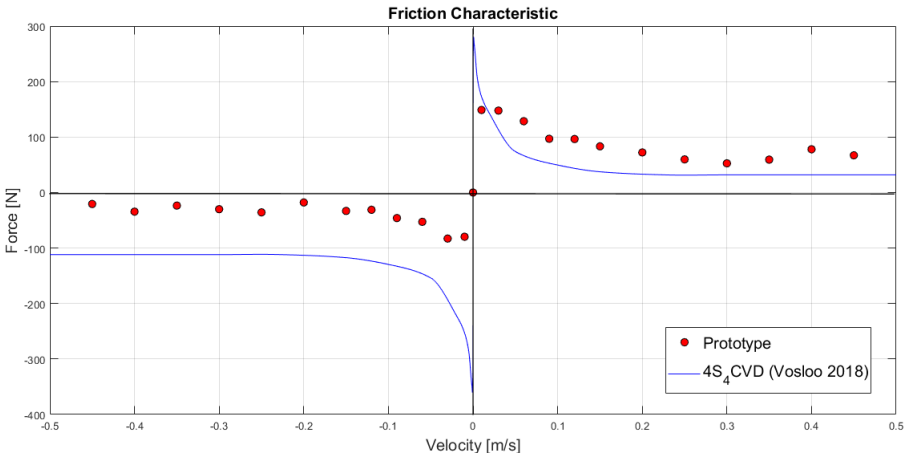

Figure 4.11. Friction characteristic of the prototype.

The friction data is presented in figure 4.11 the data measured by Vosloo (2018) is also shown for comparison. From this figure it is clear that stick slip is prominent causing static friction peaks of about a 100N for compression and 150N for rebound. As the velocity increases and the effect of the stick slip or static friction declines, the dynamic friction settles at about 30N for compression and 80N for rebound. The hydraulic seals used in the prototype has a rectangular cross section. It is therefore expected that the friction profile should be very symmetric. The slight off-set as in figure 4.11 might

be due to the fact that in compression the strut tube is well lubricated as opposed to a dry tube wall in rebound.

If the friction force magnitude is considered it is clear that the friction of the new architecture might not contribute significantly to the total strut force output. The added complexity of adding a friction model is not significant.

4.2.1 Floating piston friction characteristic

Vosloo (2018) believed that a great contributor to the friction profile of the $4S_4$ was due to the use of floating pistons, hence the consideration of the rolling diaphragms. Seeing the issues around using the rolling diaphragm and resolving the issues by reverting back to floating pistons the effect of the friction of this component can be considered.

Having pressure measurements on the gas and oil side of the floating piston makes it possible to get information regarding the friction of this component. It is expected that if the friction of the floating piston is high there will be a delay in force transfer between the gas and oil. From figure 4.12 it can be seen that this is not the case. A slight difference can be seen in the displacement range $[-80; -60]mm$. Other than this off-set no significant differences can be seen.

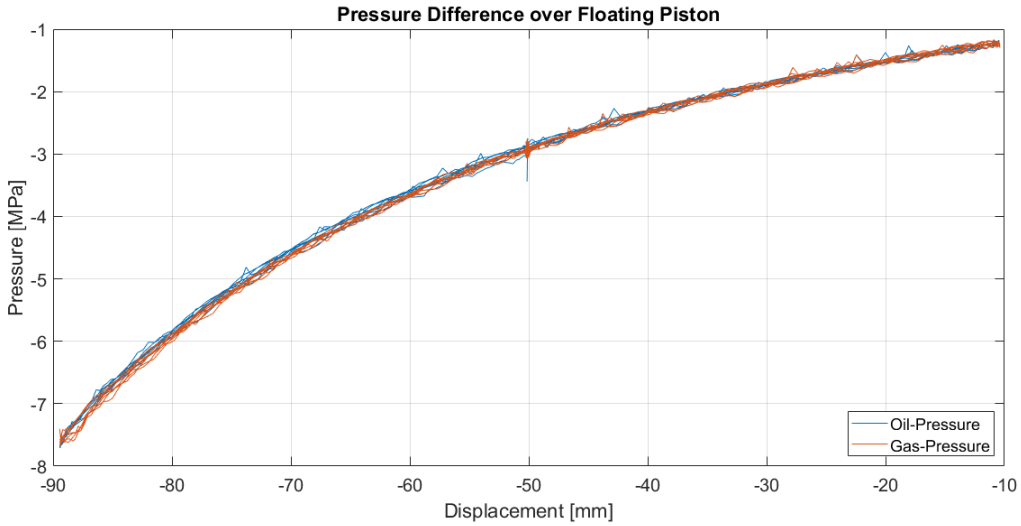

Figure 4.12. Pressure readings across the accumulator floating pistons.

From these results it is clear that the friction force of the prototype is greatly reduced by using a smaller diameter piston and that the effect of the floating piston does not have the anticipated effect on the friction characteristics as compared to the $4S_4CVD$ in figure 4.11. It is clear that the anticipated effect

of the floating piston is false and that the component of the friction profile caused by the floating piston is negligible in comparison to the effect of the piston size.

4.3 Hydro-Pneumatic Spring Model

4.3.1 Calculating accumulator pressure

The spring characteristic is determined by the pressure of the gas in the accumulators. The BWR real gas model incorporating the Energy Equation (EE) is used to calculate the pressure of the gas in the accumulators. Van der Westhuizen & Els (2015) showed that incorporating the EE with the BWR gas model gave excellent correlation with experimental data. The compressibility of the oil is also taken into consideration, making use of the experimentally determined bulk modulus presented by Els (2006).

To determine the pressure in the accumulator:
The compressibility of the hydraulic fluid is calculated with:

$$\Delta V = \frac{P \cdot V_{oil}}{\beta} \tag{4.7}$$

The compressibility is added to the displacement of the strut to determine the volume change caused by the flow rate induced by the piston movement. From this the specific volume of the gas can be calculated with the mass equal to the mass calculated by the ideal gas law for the initial state of the gas in the accumulator after it has been charged:

$$m_{gas} = \frac{P_0 \cdot V_0}{R \cdot T_{ambient}} \tag{4.8}$$

The specific volume is thus:

$$\nu = \frac{V_0 + disp \cdot A + \Delta V}{m_{gas}} \tag{4.9}$$

The flow rate of the hydraulic fluid will directly relate to the rate of change of the specific volume of the gas. Thus the rate of change of specific gas volume is calculated as:

$$\dot{\nu} = \frac{q}{m_{gas}} \tag{4.10}$$

The change in temperature can be determined by first solving equation:

$$c_v^0 = R\left[\frac{N_1}{T_g^3} + \frac{N_2}{T_g^2} + \frac{N_3}{T_g} + (N_4 - 1) + N_5 T_g + N_6 T_g^2 + N_7 T_g^3 \frac{N_8 y^2 e^y}{(e^y - 1)^2}\right] \tag{4.11}$$

with $y = \frac{N_9}{T_g}$, and then the specific heat calculated with:

$$c_v = c_v^0 + \frac{6}{T_g^3}\left(\frac{C_o}{\nu} - \frac{c}{\gamma}\right) + \frac{3c}{T_g^3}\left(\frac{2}{\gamma} - \frac{1}{\nu^2}\right) e^{\frac{-\gamma}{\nu^2}} \tag{4.12}$$

The first order differential equation to calculate the temperature update as used by Otis & Pourmovahed (1985) can now be solved. The Euler numerical integration method is used in solving this equation:

$$\dot{T}_g = \frac{T_s - T_g}{\tau} - \frac{\dot{v}}{c_v}\left[\frac{T_g R}{v}\left(1+\frac{b}{v^2}\right) + \frac{1}{v^2}\left(T_g B_0 R + \frac{2C_0}{T_g^2}\right) - \frac{2c}{v^3 T_g^2}\left(1+\frac{\gamma}{v^2}\right)e^{\frac{-\gamma}{v^2}}\right] \tag{4.13}$$

The calculated variables can now be substituted into the BWR real gas model to determine the pressure update:

$$P = \frac{RT_g}{v} + \left\{\frac{B_0 RT_g - A_0 - \frac{C_0}{T_g^2}}{v^2} + \frac{bRT_g - a}{v^3} + \frac{a\alpha}{v^6} + \frac{c\left(1+\frac{\gamma}{v^2}\right)e^{\frac{-\gamma}{v^2}}}{v^3 T_g^2}\right\} \tag{4.14}$$

The pressure of the gas in the accumulator is thus calculated and updated for every sampling period time step of a given input signal. The signal must contain the displacement and velocity of the strut. From this process the pressure can be said to be a function of 5 variables ($P_{accumulator} = f(x, \dot{x}, V_0, P_0, T_g)$). The BWR constants for nitrogen is reported in Appendix B.

4.3.2 Flow Split

Considering the discussion in section 2.5.2 and the need for flow split in modelling transients, flow split is included in the modelling of the proposed configuration.

The flow rate induced by the movement of the piston divides into the flow rates to and from each of the accumulators as illustrated in figure 2.13:

$$Q_3 = Q_1 + Q_2 \tag{4.15}$$

with Q_3 the fluid flow caused by the velocity of the strut and Q_1 & Q_2 the flow rates to accumulator 1 and 2.

Vosloo (2018), as well as Theron & Els (2007) modelled the flow split, solving for the flow split fraction with a numerical method (4^{th}-Order Runge-Kutta) in the following equation:

$$Q_3 = [(Q_{frac} \times Q_1) + (1 - Q_{frac}) \times Q_2] \tag{4.16}$$

while adhering to the mathematical constraint that constrains the pressure in the system to be equal:

$$P_1 - P_2 = 0 \tag{4.17}$$

This will force the solution to ensure that the pressures in the 2 accumulators will equalize.

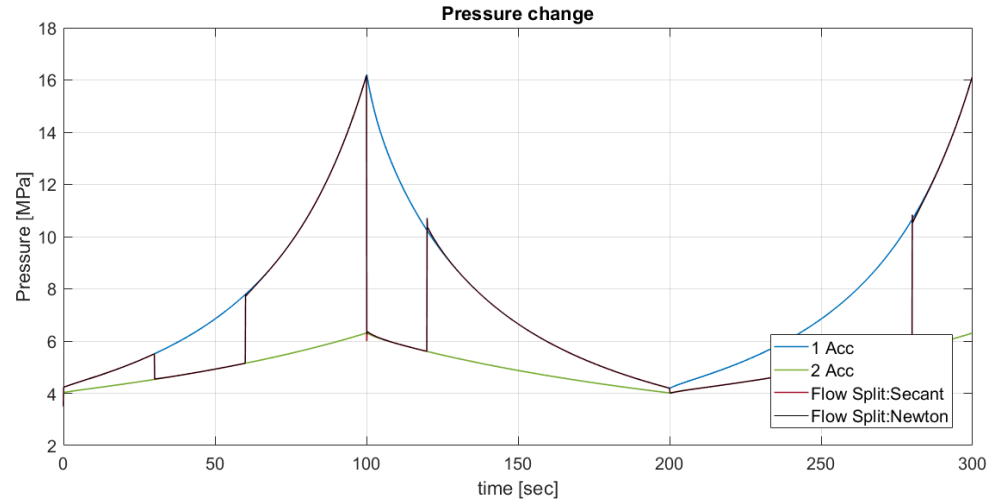

(a) Accumulator pressures.

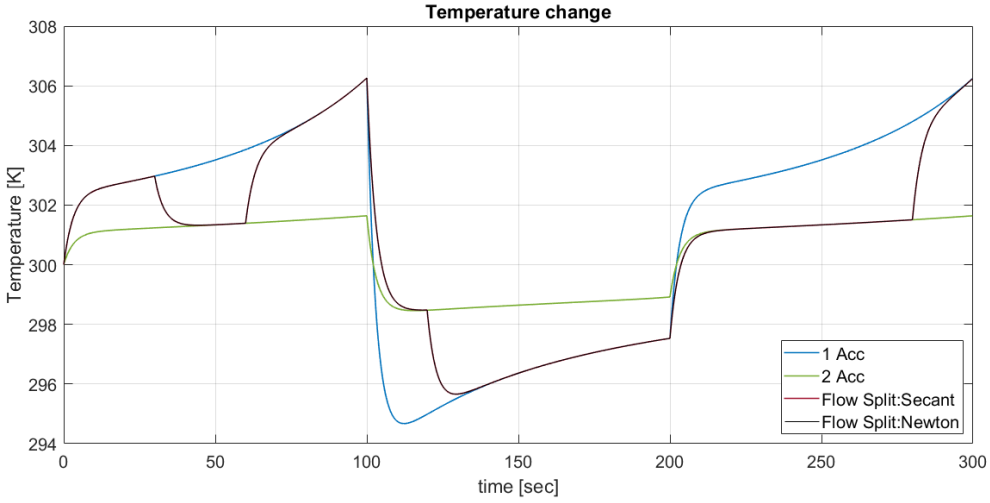

(b) Accumulator gas temperature.

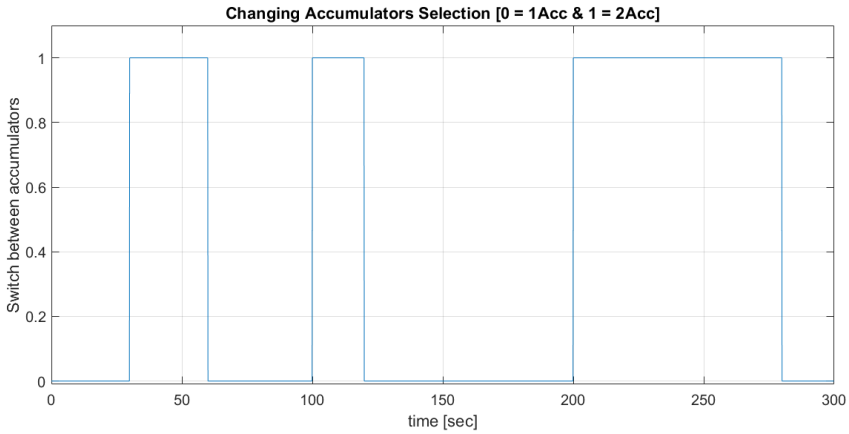

(c) Switching signal considered.

Figure 4.13. Model output considering flow split.

Vosloo (2018) reported that the 4^{th}-order Runge-Kutta method was computationally too expensive to consider flow split in simulation. Hence this numerical method was not considered. Newton's method was very stable in solving the flow split fraction. However due to the need to compute the derivative at every sampling time step this method was also to slow to consider for simulation ($13min.$ solving time to solve 10000 samples of a constant velocity input). Due to the derivative being the expensive computation, the Secant method was used, as this method does not require the derivative. Secant was not as stable in solving the flow split fraction as Newton but tremendous improvements in solving time were achieved ($0.9sec.$ solving time to solve the same 10000 samples as with Newton).

Full vehicle simulations were not yet attempted but the improvements made for solving the flow split problem, makes it possible to include flow split as a default in this model. Solution time becomes very important when the suspension model and its characteristics has to be included in full vehicle model simulations.

Supplying the model with a constant velocity input, the supply current to the flow control valve as $1.5A$ (lowest damping setting) and switching the on/off valves (response time considered to indicated instabilities clearly) between hard and soft numerous times as presented in figure 4.13(c). The results are presented in figure 4.13. From figure 4.13(a) it is clear that the Secant method solves the flow split problem quite accurately when compared to the Newton method (Some overshoot peaks can be seen for Secant that does not feature in Newton). The small deviation in accumulator pressure that is present is due to the temperature of the gas in the accumulator.

4.3.2.1 Temperature stabilization

From figure 4.13(b) a deviation can be seen in the accumulator gas temperature with the flow split. The temperature of the gas is a function of the thermal time constant used by the EE to update the temperature of the gas before employing the BWR real gas model (For this investigation consider a thermal time constant of $3.2sec.$). Hence the temperature will not immediately update. Instead, it will settle according to the time constant.

To ensure the temperature of the gas does indeed converge, the input was repeated over a longer simulation time span. A input signal was created using a constant stroking velocity of $300\frac{mm}{s}$ with a stroking length of $100mm$. In this simulation one switch was made from hard to soft and let to reach steady state. Another simulation was conducted where the valves were switched at random positions

in the simulation to determine if the temperature will converge for more complex valve switching locations. From these simulations, it was clear that the temperature does converge and hence the physics is captured well in the model. The results are presented in figure 4.14

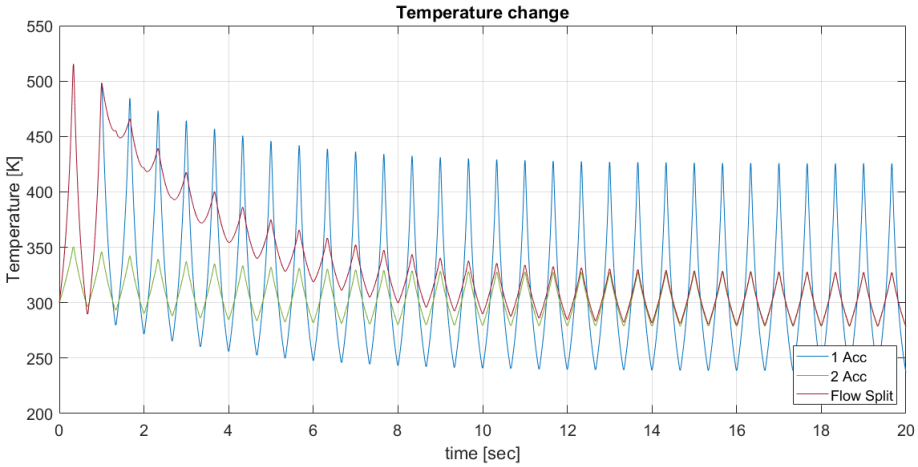

(a) One switch over

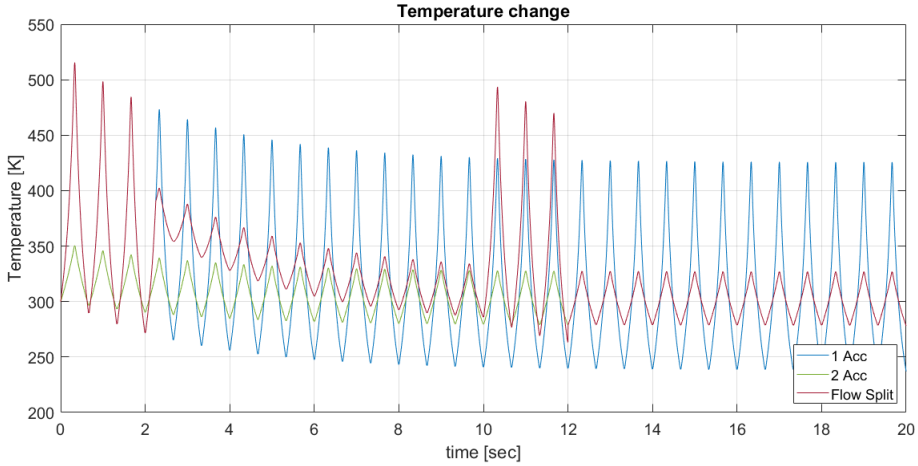

(b) Multiple switch overs

Figure 4.14. Accumulator gas temperature update.

4.3.3 Time-delay

Els (2006) performed extensive work on classifying the time delay of the SV10-24 valves, used as the on/off valves to select the gas accumulators in the proposed architecture. From this work it is clear that the time delay of the SV10-24 valves are dependent on the pressure drop over the valve and that a big initial delay is present. For this reason whenever the valves are switched in the model:

1. The total time delay is determined by the relation presented by Els (2006):

$$T = 0.4212\Delta P^2 + 0.2038\Delta P + 41.908 \tag{4.18}$$

2. This total time delay is used to create a function as depicted in figure 4.15.

3. From the sampling time that the switching took place until the last sample time in the duration of the total time delay determined. The fraction of the valve opening is determined with the function created in step 2. The pressure update of the accumulator for this duration is calculated as follows, instead of the full update:

$$P_{Accumulator}(i+1) = P_{Accumulator}(i) + frac \times P_{Accumulator}(i+1); \tag{4.19}$$

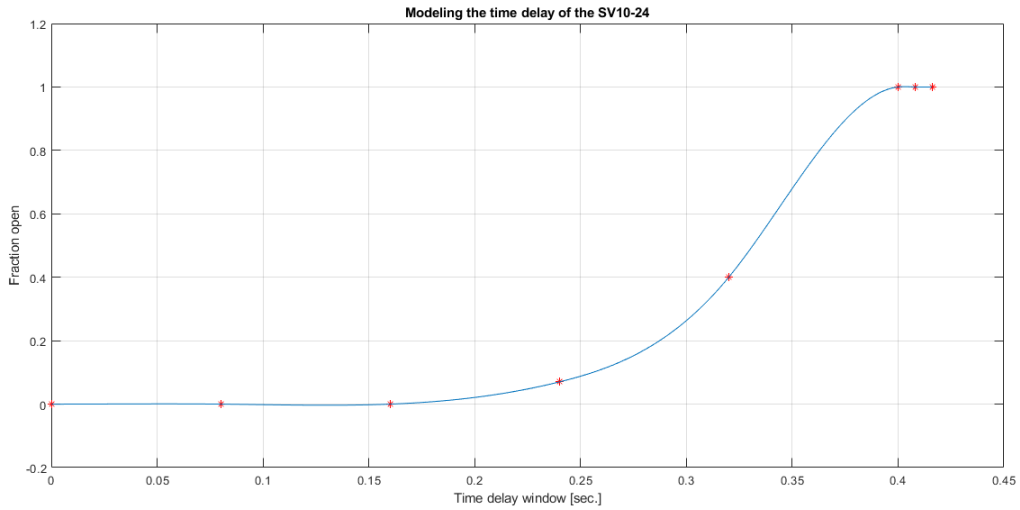

Figure 4.15. $SV10-24$ time delay model for switching the valve.

The switching of the valve will slow the response of the system down and make the dynamics of the model more stable. Hence overshoot or numerical instability for the flow split is less likely.

To show the time delay of the switching consider figure 4.16. From this figure, it is clear that the switch happened over a particular time duration and is not immediately between 2 sampling time data points. The time delay for the switching of the flow control valve is not included in the model. An adequate control circuit needs to be developed that will allow for current switching in any variation within the operating region of the valve. With such a circuit it will be possible to determine the time delay experimentally.

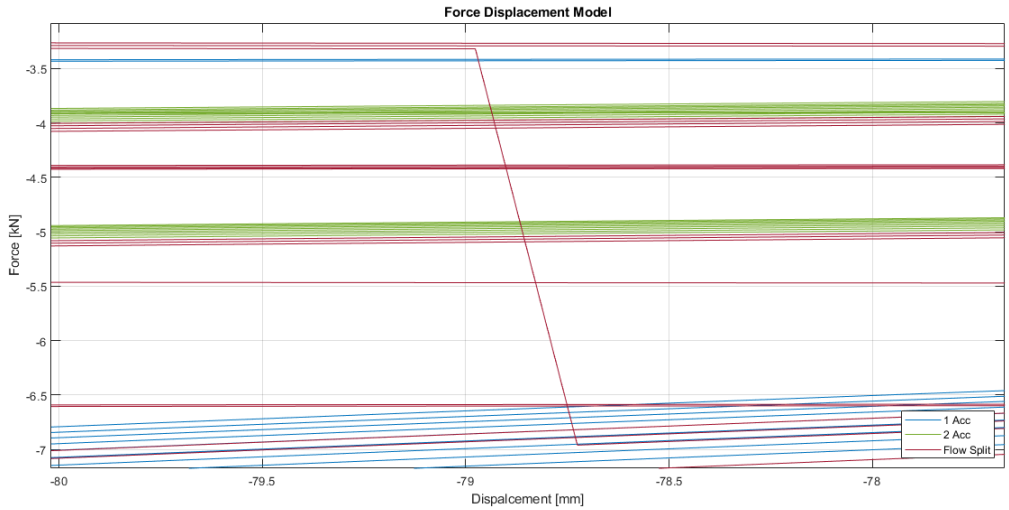

Figure 4.16. $SV10-24$ time delay demonstration.

The modelling and deeper understanding of the physics behind the individual components was considered. This allows for deeper insight into how the physics can be represented mathematically. These models can now be used in combination as considered in the following section.

4.4 Combined Model Prediction vs Experimental Data

Having a model for the pneumatic spring and a combined damping model, consisting of the blow-off valve and the flow control valve, these models can be combined to give the full force output of the prototype.

The combined model takes as input the displacement and velocity of the strut as well as the current supply to the flow control valve and the selection for opening and closing valves 1 & 2. This information is then sent to the relevant sub-models, and the force that the suspension produced is calculated as follows:

$$F_{total} = (P_{accumulator} + \Delta P_{damping}) \cdot A_{piston} \tag{4.20}$$

In order to account for the bi-directional blow-off damper and the horizontal shift of the transitions stage as well as the considerations discussed in section 4.1.4 the basic valve model is adapted as follows:

$$\left.\begin{aligned} Q &= (A_p + A_{CVD})\sqrt{\tfrac{2\cdot\Delta P}{\rho}} && P \leq P_{vfc} \\ Q &= A_v\sqrt{\tfrac{2(\Delta P - P_{vfc})}{\rho}} + Q_{Off-set} && P > P_{vfc} \end{aligned}\right\} \tag{4.21}$$

with:

- $A_p = 1.33mm^2$
- $A_{v-compression} = 5.74mm^2$
- $A_{v-rebound} = 7.55mm^2$
- A_{CVD} being the area calculated by the hermite polynomial for the supply current to the flow control valve.
- Still modelling P_{vfc} with equation 4.4.
- $Q_{Off-set} = Q_{Blow-off} - Q_{A_{P_{Blow-off}}}$
- $C_d = 0.62$ applied to A_p. The C_d values for A_{CVD} & A_v is accounted for in the calculation of the equivalent diameters from experimental data. Thus for the actual sizes these values must be multiplied with the experimentally determined C_d value.

Implementing theses changes to the damping model and comparing the model output to the experimental data for the displacement and velocity input as obtained from the feedback of the experiment yields the comparison as presented in figure 4.17. The figure presents the data for an actuation velocity of $0.5\frac{m}{s}$ to ensure that the damping effect will be prominent and because the data did not contain high frequency noise, thus filtering was not required.

The pneumatic spring characteristic can be determined by operating the actuator at a very low velocity. This will ensure that dynamic effects, such as damping, and more importantly thermal effects of the gas to have a small influence on the extracted gas spring characteristic. From figure 4.17(a) it is clear the BWR gas model with including the energy equation (with the assumption that $\tau = 6.5sec$) can predict the gas spring characteristic extremely well. The floating piston seal on the $0.16l$ accumulator of the prototype leaked, hence the presentation of only the $0.04l$ accumulator. Although the $0.16l$ accumulator could not be used in experimental work, the excellent correlation obtained as presented in figure 4.17(a) gives confidence that the modelling of the spring characteristics match the actual spring force. The prototype design allows for the independent selection of the gas accumulators by making use of the on/off valves depicted in figure 2.16. The isothermal prediction for three of the four capable spring characteristics is presented in figure 4.18. The fourth characteristic is due to the compressibility of the oil when both accumulators is closed off. This is an extremely stiff linear characteristic determined by the Bulk modulus of the oil.

Figures 4.17(b) - 4.17(d) presents the comparison for changing the damping setting for the same velocity input. From these figures it is clear that the damping increases the hysteresis loop as expected seeing that an increase in damping will increase the dissipation of energy. Notice that the hysteresis loop has different magnitudes on either side of the midpoint of the experiments, which is caused by the difference in rebound and compression damping forces.

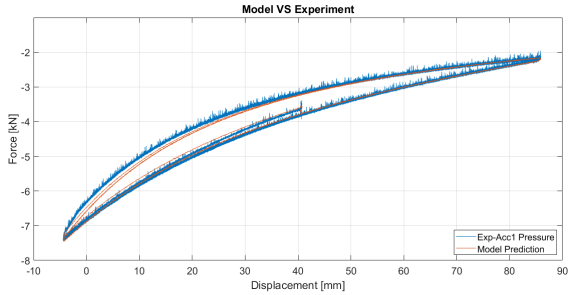

(a) Accumulator gas prediction.

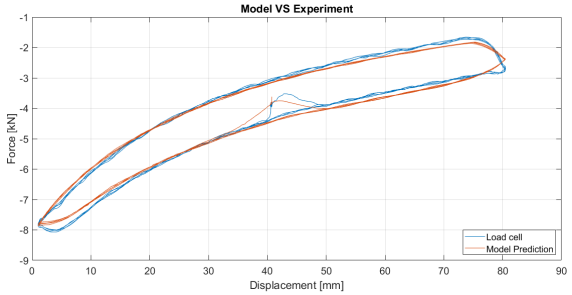

(b) Lowest damping $(1.5A)$ @ $0.5\frac{m}{s}$.

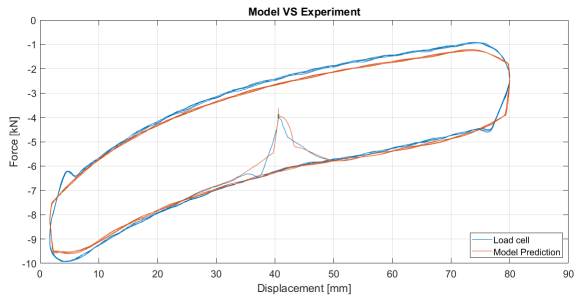

(c) Medium damping $(0.4A)$ @ $0.5\frac{m}{s}$.

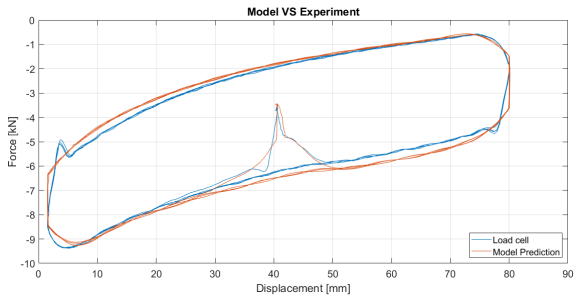

(d) Highest damping $(0A)$ @ $0.5\frac{m}{s}$.

Figure 4.17. Updated model comparison with experimental data.

Overall the model performs well in predicting the force as produced by the prototype. The model however lacks in the prediction of the transition between rebound and compression damping as expected from the discussion of the complex flow when the blow-off valve opens. The transition stages also include dynamic effects such as the inertia of the components at the turn around point and the actuator control that can overshoot or undershoot at these points. The model presented here did not include the extracted friction profile. Due to the low dynamic friction force the effect of including friction in the model seemed minimal. However it is clear that there is a small difference between the model prediction and the measured force. The friction might reduce this but a bigger effect will be achieved by increasing the accuracy of the polynomial prediction for the CVV. The polynomial was fitted to limited experimental data from Vosloo (2018). Figure 4.2 shows how the limited data contributed to a prediction that is slightly off. Having safe operation due to the blow-off valve a well

defined range of damping measurements can be obtained experimentally to improve the accuracy of the polynomial prediction as presented in equation 4.3.

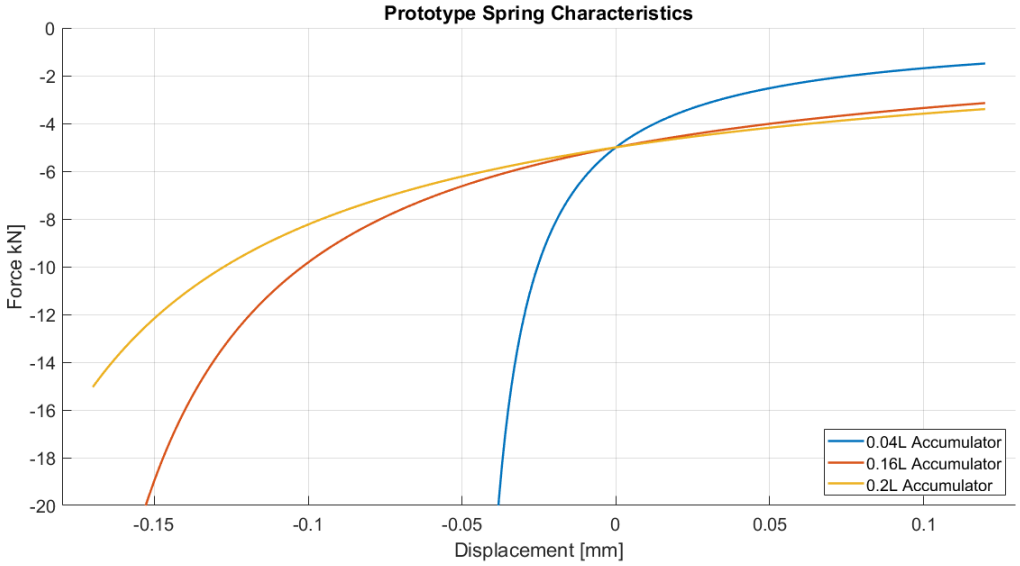

Figure 4.18. Isothermal predictions of the capable spring characteristics .

This chapter showed that by using a physics based mathematical modelling approach a deeper conceptual understanding of the different components and their functioning is obtained. The proposed damping combination, bow-off valve in parallel with the flow control valve, was modelled by adapting the basic valve model proposed by Dixon (2007) in accordance to the physical phenomena seen from experimental data. It was shown that the reduced friction of the prototype made it possible to exclude friction from the mathematical model and that the anticipated effect of the floating piston's friction false. Modelling the spring characteristics of a hydro-pneumatic spring is a well understood topic from literature. The spring characteristics of this model includes temperature updates by employing the EE with the use of the BWR real gas model to calculate the accumulator gas pressures. Improvements made in simulation time makes it possible to include flow split as default. Other consideration included in the spring model includes the time delay of the on/off valves as well as the compressibility of the oil.

5. Conclusions and Recommendations

5.1 Conclusions

From literature, the need for a semi-active suspension system that can solve the ride comfort *vs* handling compromise has been realized. The potential benefit of variable damping in such a system was also determined. The potential of a hydro-pneumatic semi-active suspension system with continuously variable damping as well as four discrete spring characteristics is high, especially if the spring and damping characteristics can be changed within an acceptable response time. Literature also provided a background of the complexity needed for modelling such a system to represent a physical unit mathematically.

The $4S_4$ platform developed by Els (2006) not only solved the compromise between ride comfort and handling in suspension design but introduced the possibility of improving the vehicle dynamics even further. In an attempt to utilize the potential benefits of continuous variable damping Vosloo (2018) investigated an architecture of the original $4S_4$ that tried to realise continuous variable damping. Building on the knowledge gained from Vosloo's investigation and literature a new architecture was proposed that will allow for a semi-active hydro-pneumatic suspension system with continuous variable damping.

A prototype of the new configuration was designed and manufactured (not covered in the scope of this document) to mimic the proposed configuration. The prototype allowed for experimental validation of the mathematical model and to test the feasibility of the proposed configuration. The proposed configuration and hence the prototype was capable of achieving the optimal handling characteristic as well as an extremely low characteristic required for ride comfort while allowing for the variability in between these 2 states.

The physics based model incorporates: compressibility of the oil, thermal properties of the gas, response time of the on/off valves and tailored flow principals through the orifice combination used. The model is capable of predicting the force output of the prototype with good accuracy and can be used in the development and improvement for suspension components to manipulate the vehicle dynamics to ensure a safe, but comfortable ride. The proposed configuration also made the realisation

of controllable continuous variable damping possible within the semi-active hydro-pneumatic design envelope.

5.2 Recommendations for Future Work

The proposed configuration and the developed prototype allow for numerous opportunities to be explored. These opportunities range from improvement of the prototype to the advanced control of vehicle dynamics. The ultimate goal is to achieve full vehicle implementation. However before this can be realized there are some interim steps that will ensure a greater possibility of success:

1. **Response time:**

   Response time of the on/off valve is well documented by Els (2006). Vosloo (2018) did present data on the response time of the proportional flow control valve. It is uncertain whether this data represents the full response time of the proportional valve. The response time of the proportional valve needs to be confirmed. This will allow for individual component assessment but in the bigger picture the full system response need to be measured and modelled.

2. **Thermal time constant:**

   The thermal time constant for the full model prediction was varied iteratively to obtain the correlations as presented in section 4.4. This was done in an educated manner between the known thermal constants from Els (2006) and Vosloo (2018). The thermal time constant needs to be determined experimentally for completeness sake of the model.

3. **Blow-off mechanism:**

   With the current design the blow-off mechanism was seen to be on/off in operation with some undesired flutter induced in the opening region. This means that the gradual transition between 2 characteristics could not be achieved. This has the possibility to introduce an unwanted damping characteristic if the design is not considered carefully. A deeper investigation into the blow-off valve opening flow and the effect that different opening mechanisms can have on the damping characteristic will ensure a blow-off valve design that can be described mathematically and eliminate any uncertainties in operation.

4. **Ride height actuation:**

   The current prototype makes provision for active ride height control through the use of 2 proportional flow control valves. In full vehicle implementation the adjacent units can be configured to act as a hydraulic anti-roll bar. Hence giving the ability of not only controlling the ride height but also to actively manipulate roll characteristics of the vehicle. This aspect of the

prototype was not considered experimentally or mathematically. The possibilities, drawbacks and requirements for this aspect of the prototype needs to be investigated if the potential is to be realized.

5. **Control:**

   Els (2006) showed that with a simple controlling strategy the $4S_4$ was capable of negating the compromise between ride comfort and handling. For the proposed configuration to really perform at its full potential, a good control strategy, taking into account the large variation in suspension requirements need to be implemented. Hence the need for the development of a control strategy that will ensure the correct component (spring force, damping, ride height) is controlled in an adequate manner to ensure the required vehicle dynamics is achieved.

6. **Full vehicle model:**

   Having a validated model for the suspension forces and investigating the best control strategy to manipulate the vehicle dynamics will require a validated full vehicle model. This model will aid in the development and improvement of the platform and ensure that considered changes can be weighed against the perceived ride improvements and added complexities. A validated vehicle model can also be used to tailor the damping characteristics to the vehicle considered e.g. what is the optimal relation between compression and rebound damping? How does the manipulation of the damping affect the ride comfort and handling capabilities.

7. **Design iteration:**

   Knowing that the configuration of components will function in a desirable manner and having simulation results for optimal operation the prototype design needs to go through a design iteration phase. The design iteration phase needs to address questions such as:

   - What is the best packaging for the configuration?
   - How can the design be adapted to ensure fast but accurate manufacturing?
   - Is it possible to reduce design complexity to reduce the possibility of components failing?
   - What is the expected life cycle that must be accounted for? etc.

References

Ahmed, M. R., Yusoff, A. R. & Romlay, F. R. M. (2019), 'Numerical investigation of continuous damping of the semi-active suspension system for passenger car', *IOP Conference Series: Materials Science and Engineering* **530**, 012014.

Alonso, M. & Comas, . (2006), 'Modelling a twin tube cavitating shock absorber', *Proceedings of the Institution of Mechanical Engineers, Part D: Journal of Automobile Engineering* **220**(8), 1031–1040.

Beghi, A., Liberati, M., Mezzalira, S. & Peron, S. (2007), 'Grey-box modeling of a motorcycle shock absorber for virtual prototyping applications', *Simulation Modelling Practice and Theory* **15**(8), 894–907.

BritishStandardsInstitution (1987), *British Standard guide to measurement and evaluation of human exposure to whole-body mechanical vibration and repeated shock*.

Castellani, F., Scappaticci, L., Bartolini, N. & Astolfi, D. (2017), 'Numerical and experimental investigation of a monotube hydraulic shock absorber', *Archive of Applied Mechanics* **87**(12), 1929–1946.

Dixon, J. C. (2007), *The shock absorber handbook*, second edn, John Wiley.

Duym, S. W. (2000), 'Simulation tools, modelling and identification, for an automotive shock absorber in the context of vehicle dynamics', *Vehicle System Dynamics* **33**(4), 261–285.

Els, P. S. (2006), The Ride Comfort vs. Handling Compromise for Off-Road Vehicles., PhD thesis.
URL: *https://repository.up.ac.za/handle/2263/26302*

Els, P. S. & Grobbelaar, B. (1993), 'Investigation of the time- and temperature dependency of hydro-pneumatic suspension systems', *SAE Technical Paper Series* .

Gillespie, T. (1992), *Fundumentals of Vehicle Dynamics*, Society of Automotive Engineers INC.

Grobler, J. F. (2016), Multi-stage hydro-pneumatic suspension system through the use of magneto-rheological (valves). (unpublished), Master's thesis.
URL: *https://repository.up.ac.za/handle/2263/66198*

Heymans, G. S. (2017), Development of a magneto-rheological (mr) equipped semi-active suspension system for off-road vehicles. (unpublished), Master's thesis.
URL: *https://repository.up.ac.za/handle/2263/66204*

Jacobsen, R. T. & Stewart, R. B. (1973), 'Thermodynamic properties of nitrogen including liquid and vapor phases from 63k to 2000k with pressures to 10,000 bar', *Journal of Physical and Chemical Reference Data* **2**(4), 757–922.

Jugulkar, L. M., Singh, S. & Sawant, S. M. (2016), 'Analysis of suspension with variable stiffness and variable damping force for automotive applications', *Advances in Mechanical Engineering* **8**(5), 1–19.

Lang, H. H. (1977), A study of the characteristics of automotive hydraulic dampers at high stroking frequencies, PhD thesis.

Leser, C., Renner, T. E. & Salmon, D. C. (2002), 'Accurate shock absorber load modeling in an all terrain vehicle using black box neural network techniques', *SAE Technical Paper Series* .

Lichtarowicz, A., Duggins, R. K. & Markland, E. (1965), 'Discharge coefficients for incompressible non-cavitating flow through long orifices', *Journal of Mechanical Engineering Science* **7**(2), 210–219.

Mcgreehan, W. F. & Schotsch, M. J. (1988), 'Flow characteristics of long orifices with rotation and corner radiusing', *Journal of Turbomachinery* **110**(2), 213–217.

Meeser, R. F. (2015), Magneto rheological (mr) damper design for off-road vehicle suspension with flow blocking ability. (unpublished), Master's thesis.
URL: *https://repository.up.ac.za/handle/2263/45961*

Otis, D. R. & Pourmovahed, A. (1985), 'An algorithm for computing nonflow gas processes in gas springs and hydropneumatic accumulators', *Journal of Dynamic Systems, Measurement, and Control* **107**(1), 93–96.

Reybrouck, K. (1994), 'A non linear parametric model of an automotive shock absorber', *SAE Technical Paper* .

Savaresi, S., Poussot-Vassal, C., Spelta, C., Sename, O. & Dugard, L. (2010), *Semi-Active Suspension Control Design for Vehicles*, 1 edn, Butterworth-Heinemann.

Segel, L. & Lang, H. H. (1981), 'The mechanics of automotive hydraulic dampers at high stroking frequencies', *Vehicle System Dynamics* **10**(2-3), 82–85.

Sha, S., Wang, Z. & Du, H. (2020), 'Research on performance of vehicle semi-active suspension applied magnetorheological damper based on linear quadratic gaussian control', *Noise and Vibration Worldwide* **51**(7-9), 119–126.

Theron, N. & Els, P. (2007), 'Modelling of a semi-active hydropneumatic spring damper unit', *International Journal of Vehicle Design* **45**(4), 501.

Thoresson, M. J. (2007), Efficient gradient-based optimization of suspension characteristics for an off-road vehicle (Under exam.), PhD thesis.
URL: *https://repository.up.ac.za/handle/2263/26984*

Van den Bergh, J. S. (2014), Effects of friction and gas modelling on vehicle dynamics simulation. (unpublished), Master's thesis.
URL: *https://repository.up.ac.za/handle/2263/56116*

Van der Westhuizen, S. F. & Els, P. S. (2015), 'Comparison of different gas models to calculate the spring force of a hydropneumatic suspension', *Journal of Terramechanics* **57**, 41–59.
URL: *www.sciencedirect.com*

Vosloo, A. G. (2018), Characterization,modeling and control of a hydropneumatic semi-active suspension system with continuous variable damping. (unpublished), Master's thesis.

A. Experimental Blow-off valve Assembly Drawing

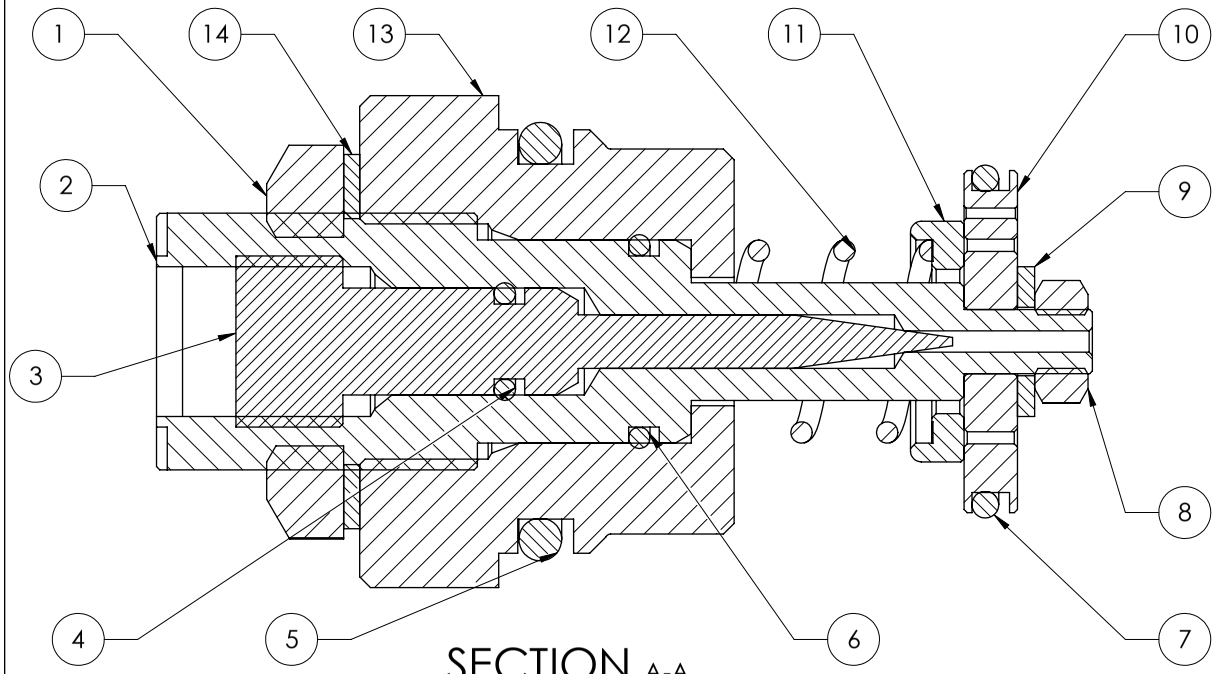

SECTION A-A

SCALE 2 : 1

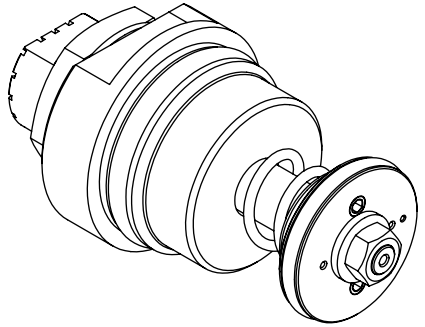

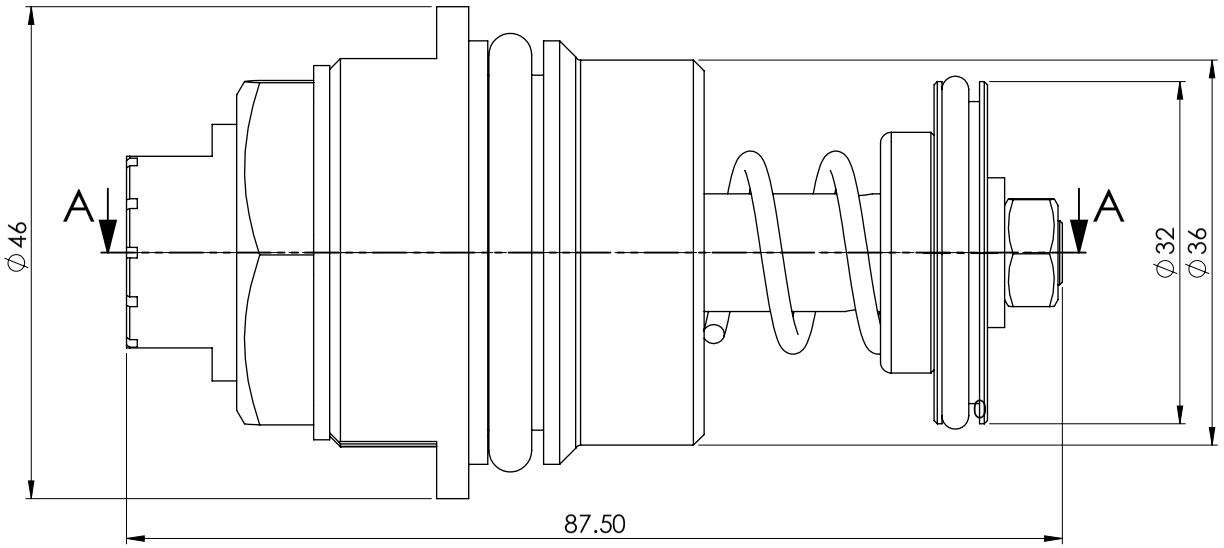

1	1	M22x2.5 HALF NUT
2	1	SHAFT
3	1	NEEDLE VALVE
4	1	7MM ORING (DIA 2MM)
5	1	33 MM ORING (DIA 4 MM)
6	1	16 MM ORING (DIA 2 MM)
7	1	28 MM ORING (DIA 2.5 MM)
8	1	M6 x 1 NUT
9	1	M6 WASHER
10	1	ORIFACE PLATE
11	1	BLOCKING PLATE
12	1	LANDY SPRING
13	1	DAMPER PLUG
14	1	M22 WASHER

1. I understand what plagiarism is and am aware of the University's policy in this regard.
2. I declare that this drawing is my own original work.
3. I have not used another student's past work to hand in as my own.
4. I have not allowed, and will not allow, anyone to copy my work with the intention of passing it off as his or her own work.

_____

TOLERANCES	
FROM - TO	+/-
0 - 6	0.1
6 - 30	0.2
30 - 100	0.3
100 - 300	0.5
300 - 1000	0.8
1000 - 3000	1.2
3000 - PLUS	2.0
ANGLES	1°

ITEM NR / ITEM NO	AANTAL / QUANTITY	BESKRYWING / DESCRIPTION	MATERIAAL / MATERIAL	ONDERDEEL NR / PART NR

VAN / SURNAME	DE WET	VOORLETTERS / INITIALS B	TITEL / TITLE DAMPER PACK
STUDENTE NO / STUDENTE NR	u15334440	RIGTING / DISCIPLINE M	TEKENING NR / DRAWING NR
PROJEKSIE / PROJECTION	UNIVERSITEIT VAN PRETORIA / UNIVERSITY OF PRETORIA	A3	SKAAL / SCALE 1:1 — DATUM / DATE 2019/09/06

C:\Users\user\Documents\Benjamin\Coarse_Work\MSS_780\Blowoff_Valve\Experiment_Valve\Experiment_DamperPack Last saved 23 August 2019 07:25:51

VOLTOOI TITELBLOK IN SWART INK/COMPLETE TITLEBLOCK IN BLACK INK

B. BWR constants for Nitrogen

Constants for the BWR equation (Els & Grobbelaar (1993)):

- $a = 0.115703387 \left[\left(\frac{m^3}{kg}\right)^3 \frac{N}{m^2}\right]$
- $\mathrm{A}_0 = 136.0474619 \left[\left(\frac{m^3}{kg}\right)^3 \frac{N}{m^2}\right]$
- $\equiv 2.96625 \times 10^{-6} \left[\left(\frac{m^3}{kg}\right)^3\right]$
- $B_0 = 0.001454417 \left[\frac{m^3}{kg}\right]$
- $c = 7.3806143 \times 10^{-5} \left[\left(\frac{m^3}{kg}\right)^3 K^2 \frac{N}{m^2}\right]$
- $C_0 = 1.0405873 \times 10^{-6} \left[\left(\frac{m^3}{kg}\right)^3 K^2 \frac{N}{m^2}\right]$
- $\alpha = 5.863972 \times 10^{-9} \left[\left(\frac{m^3}{kg}\right)^3\right]$
- $\gamma = 6.7539311 \times 10^{-6} \left[\left(\frac{m^3}{kg}\right)^2\right]$
- $R = 296.797 \left[\frac{J}{kgK}\right]$

Constants for the calculation of the IG specific heat capacity of Nitrogen (Jacobsen & Stewart (1973)):

- $N_1 = -735.210$
- $N_2 = 34.224$
- $N_3 = -0.557648$
- $N_4 = 3.5040$
- $N_5 = -1.7339 \times 10^{-5}$
- $N_6 = 1.7465 \times 10^{-8}$
- $N_7 = -3.5689 \times 10^{-12}$
- $N_8 = 1.0054$
- $N_9 = 3353.4061$
- $y = \frac{N_9}{T}$